Improved Seal Design Based On Minimizing Strain Energy

A THESIS
SUBMITTED TO THE FACULTY OF THE GRADUATE SCHOOL
OF THE UNIVERSITY OF MINNESOTA
BY

Daniel Alexander Matus

IN PARTIAL FULFILLMENT OF THE REQUIREMENTS
FOR THE DEGREE OF
MASTER OF SCIENCE

Barney E. Klamecki, PhD.

June, 2010

Acknowledgements

I would like to express my sincere thanks to my graduate advisor, Professor Barney Klamecki of the Department of Mechanical Engineering, for his advice and assistance with this research, and for his consistent and valuable guidance throughout my graduate career.

I would also like to thank contributing members of the Center for Compact and Efficient Fluid Power, a National Science Foundation Engineering Research Center, for funding this work, as well as for providing me with outlets to share my research findings with others in the fluid power area, and for continuously exposing me to opportunities for further learning relating to fluid power.

Thanks to Precision Associates Inc. of Minneapolis, Minnesota, for their generosity in sharing time and sample materials. These donations led to an improved understanding of the nature of sealing materials, which proved very beneficial to this research.

Thanks to RT Dygert of Minneapolis, Minnesota, for the donation of o-rings that were used in the development of my own experimental o-ring samples that helped to validate and further demonstrate the concepts behind this research.

Dedication

I dedicate this work to my wonderful parents, Petie and José, who have given me nothing but unconditional love, support, and encouragement throughout my life.

Abstract

Minimizing the strain energy in an o-ring seal has been identified as a mode of improving its useful lifetime. The intent of this research was to manipulate the strain energy content in o-ring seals by varying material properties and material behavior over the cross-section of the o-ring.

O-ring designs were developed that contained regions of modified material properties referred to as insets. These o-ring designs incorporating insets were evaluated numerically to determine the effects that the inset's stiffness, size, and placement, had on the strain energy content and maximum sealing pressure of the o-ring design. Achievements included the development of o-ring designs that demonstrated lower strain energy content than a baseline design made of a single homogeneous material.

Experimental o-rings were created using commercially available materials. Compression set and compression stress relaxation experiments were conducted. Performance of new o-ring designs including insets made of a softer material than the main o-ring was compared to baseline single material o-rings. Improved sealing performance was demonstrated by a decreased rate of sealing force decay over time, and by decreased compression set, for the new o-ring designs proposed.

With the improved sealing force retention rate seen in the experimental o-ring designs, typically there was a lower sealing force than baseline single material designs. Materials with strain-stiffening behaviors were incorporated into theoretical o-ring designs. Numerical simulations showed the usefulness of these materials in controlling the strain energy content in o-ring seals while balancing this improved stored energy state with maintaining adequate sealing capabilities. Materials with time-dependent adaptive-stiffening were also proposed, and their usefulness was demonstrated in aiding sealing pressure retention over time.

Contents

List of Tables

List of Figures

1. Introduction

Mechanical seals are essential components of fluid power systems and any other system where a working fluid needs to be contained. The seal's main functions are to maintain the pressure of a working fluid and to prevent fluid leakage from high to low pressure regions. Seals are generally manufactured from rubber materials, or elastomers, which are easily deformable due to their low stiffness and highly elastic nature.

One of the geometrically simplest and most widely used types of seal is the o-ring. The standard o-ring has a circular cross-section of a constant diameter, and forms a constant diameter torus. It is well suited for many standard applications as its installation is generally simple, and it is particularly easy to manufacture when compared to other seals with varying geometric complexity. The o-ring geometry is well-suited for static as well as dynamic applications, i.e. rotary or reciprocating parts.

A typical o-ring application is shown in Figure 1. O-rings are installed in a groove machined into a gland made of a very rigid material, and a second gland typically compresses the seal 15-25% in a standard application. To compress the o-ring, a sealing force, F_{SF}, is applied. Internal stresses in the sealing material cause reaction forces on the restraining glands. These reaction forces over the contact area at the seal-gland interface result in a seal-gland contact pressure or sealing pressure, P_{CP}. After compression in the sealing application, a working fluid will begin to exert an additional pressure, P_{WF}, on the o-ring. A successful seal design results in a contact pressure greater than the pressure of the working fluid and guarantees no leakage of the working fluid.

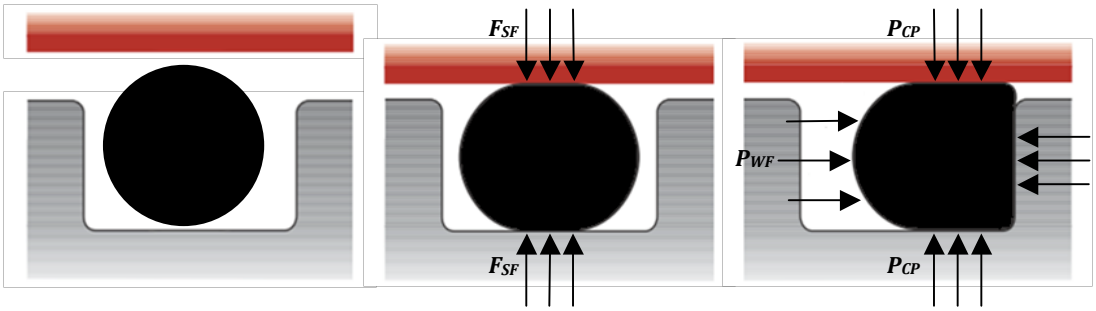

Figure 1: O-ring Application
Left: o-ring before compression. Middle: compressed o-ring after installation. Right: Pressurized working fluid exerts additional forces on the o-ring. Dichtomatik. [1]

Different applications produce different types of seal failures. Modes of o-ring failure can be related to 1) mechanical, thermal, or chemical effects, 2) human error, e.g. improper design or installation damage, or 3) elastomer properties, e.g. improper rubber curing or inherent elastomer properties. Common modes of o-ring failure are presented in Figure 2.

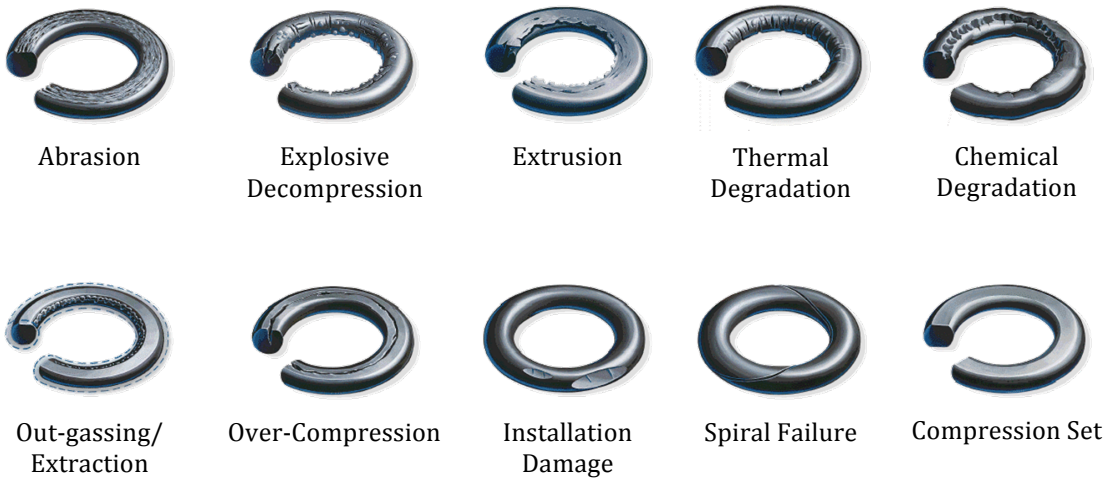

Figure 2: Modes of O-ring Failure
Abrasion and extrusion result from wear and physical motion. Thermal and chemical degradation can occur in a harsh operating environment. Installation damage can cause an o-ring to fail prematurely, while over-compression and spiral failure can be attributed to poor sealing system design. Compression set represents an irreversible change in the o-ring seal because of inherent elastomer properties, and causes a loss of sealing force over time. Allorings.com [2].

While low stiffness and highly elastic properties of elastomers lend them to be excellent candidates for sealing applications, they have the inherent property that when held under

strain for a prolonged period of time, whether compressive or tensile, there are changes at the molecular level that result in permanent deformation. Due to the onset and growth of permanent deformation, even in the absence of catastrophic failure or a harsh operating environment (e.g. extreme temperatures, chemically reactive working fluids,) sealing effectiveness degrades over time-in-use. Permanent deformation results in compression stress relaxation and a loss of sealing pressure over time. After compressive forces are removed from the seal, the material is unable to rebound to its original dimensions and geometry, and the extent of permanent deformation is defined as compression set.

Since seals are such critical components of fluid power systems, the loss of sealing effectiveness over time due to permanent deformation is highly undesirable. There exists a need to fully understand the nature of elastomer materials and determine ways of decreasing permanent deformation in seals.

In this research, new o-ring designs that aim to lessen the amount of permanent deformation of seals in-use were investigated. The approach to seal design was to modify material properties and behavior across the seal cross-section. In the following sections, background information on elastomer materials useful for this research is presented. A literature review of elastomers in sealing applications is presented, and the specific problem of seal design based on minimizing the strain energy content in the seal is described in further detail.

2. Background

2.1. Background

2.1.1. Elastomers

Interestingly, o-rings and other elastomer seals are different from many mechanical components that engineers and designers encounter, as they must deform to function properly. Elastomers possess a material structure that causes them to be very elastic. Elastomers are made of long polymer chains that cross-link during the curing process. This cross-linking process determines the shape and strength of a rubber part. The softness and elasticity of an elastomer material is caused by the ability of these long chains to reconfigure themselves in order to distribute an applied stress throughout the body. The polymer cross-linking allows the material to return to its original shape after a small strain or stress is applied for a short period of time. However, elastomers are amorphous polymers, and are essentially highly condensed and highly viscous fluids. In this respect, elastomers exhibit viscoelastic behavior, which means that in response to an applied deformation, the reaction is both elastic – i.e. energy stored, and viscous – i.e. energy dissipated over time.

For relatively small strains, ≤25%, conventional elasticity analysis can provide a good approximation of elastomeric behavior. Conventional elasticity assumes materials are isotropic, and exhibit linear stress-strain behavior. For larger deformations, elastomers exhibit highly nonlinear stress-strain behavior, thus for engineering and design, it is convenient to approach the modeling of elastomeric behavior through the use of hyperelastic material models. Hyperelastic materials are perfectly elastic materials whose stress-strain behavior is described by a strain energy density function, W, which will be described in detail in Section 6.1. Linear material models cannot adequately predict the behavior of hyperelastic materials.

2.1.2. Material Properties

The common material properties used to describe elastomeric materials for small strain applications are the bulk modulus, K, shear modulus, G, elastic modulus, E, Poisson's ratio, ν,

and hardness. The bulk modulus describes the material's resistance to volumetric compression due to an applied pressure. The shear modulus describes the material's resistance to a simple shearing stress. The material's elastic modulus is a measure of its resistance to a uniaxial tensile deformation. Experimentally, these values are defined as the slope at a given point of the material's stress-strain response curve corresponding to each type of load. From Chou and Pagano [5], analytically, all three parameters are related by,

$$E = \frac{9KG}{3K + G}.$$

Poisson's ratio is defined as the ratio of a lateral strain to a perpendicular longitudinal strain. From [5], a material's Poisson's ratio is also related to its bulk and shear moduli by,

$$\nu = \frac{3K - 2G}{2(3K + G)}.$$

Elastomers exhibit very high values of K, on the order of 1 to 2-GPa, whereas they exhibit very low values of G, on the order of 0.5 to 5-MPa. Therefore, the Poisson's ratio, ν, approaches values near 0.5, which implies that like liquids, they are nearly incompressible.

The hardness of a material is a measure of its resistance to an imposed indentation. Hardness is typically quantified by a test measuring the depth of indentation made on the surface of the material by a standard indenter. There are different hardness tests (e.g. Shore, Brinell, Rockwell, etc.) that vary the shape and size of the indenter, as well as the speed of indentation, depending on the material being tested. The Shore A hardness scale is commonly used in the United States of America to describe elastomer and polymer hardness. In this test, a 1.1 to 1.4-mm diameter hardened steel rod with a ball-end is applied with a force of 8.064-N. The depth of the indenter is measured after the load has been applied for 15-seconds, and the value is correlated to a scale from 30 to 95 points, where 95 represents the hardest materials.

Hardness is often the preferred technical specification of sealing materials in industrial applications, and is referred to as the durometer. However, when conducting structural analyses via analytical or numerical simulations, the elastic modulus is the relevant material property. A useful approach is to consider a material's elastic modulus as an intrinsic property, whereas hardness is only an engineering measurement, thus an extrinsic property. This means that the nature of the test performed affects the results and measurements. Though increasing values of elastic modulus often lead to an increase in measured hardness, there is no direct relation between the two properties.

2.1.3. Compression Stress Relaxation and Compression Set

Since elastomers are viscoelastic materials, when strained for a period of time, the material structure undergoes a combination of reversible and irreversible processes, and overall, the material's stored energy will continuously decrease over time under strain. Reversible effects involve the motion of polymer chains to new configurations to accommodate the strained state. Irreversible effects occur as the material attempts to restructure itself to a lower energy configuration for the strained state. This reconfiguration is caused by the slippage and breakage of molecular entanglements and cross-links, and by the formation of new covalent bonds. See Figure 3. These molecular reconfigurations occur very rapidly at the onset of strain, but slow greatly over time.

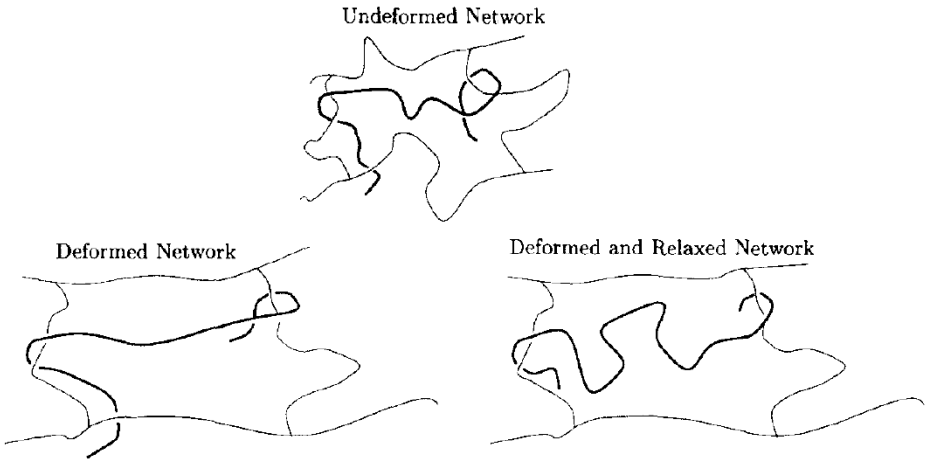

Figure 3: Cross-link Network After Permanent Deformation
Simplified representation of permanent deformation. The free polymer chain relaxes in the deformed state, and does not return to its original shape when deformation is removed [6].

This molecular reconfiguration and decreasing energy state that occurs at a fixed strain results in decreased stresses in the material over time. This phenomenon is known as compression stress relaxation. The stress relaxation phenomenon is often modeled as a logarithmic decay. Compression stress relaxation is an important phenomenon in relation to the long-term performance of o-rings. Seals in operation experience a constant compression, and the loss of sealing pressure, which is directly related to stress relaxation, causes a loss of sealing effectiveness. A related phenomenon to stress relaxation is creep. If an elastomer material experiences a constant stress for a period of time, the material's geometry will gradually succumb to the applied strain, and a continuous deformation will be observed over time. This phenomenon is not immediately relevant to standard sealing applications where seal deformation remains constant while in-use.

Compression set is a measure of stress relaxation, and is defined with respect to the degree of a material's recovery to its original dimensions post-strain. There are two ways to calculate compression set. The first is used in applications where a constant stress is applied to a material, and the second is used when a constant strain is applied to a material, and is relevant for seals subjected to a fixed deformation. For constant strain, compression set of an o-ring seal is defined as,

$$CS = \frac{d_o - d_f}{d_o - d_c} \times 100\%,$$

where d_o is the original cross-section diameter, d_c is the height of the o-ring in use, i.e. during compression, and d_f is the final recovered height of the o-ring after it is released from compression.

In essence, it is a measurement of the elastic to viscous components of an elastomer's response to a given strain. It is important to note that while stress relaxation and compression set typically both increase with increasing amounts of compression, and increasing length of time of compression, there is no direct relationship between the two phenomena. This is due to the fact that both phenomena are material-dependent,

dependent on the rate of applied deformation, and can vary with the type of testing conditions.

2.1.4. Strain Energy

Strain energy has been demonstrated to be a parameter in a seal's rate of stress relaxation and the onset and growth of compression set. Minimizing strain energy in a seal has been identified as a mode of reducing these phenomena, and thus increasing the useful lifetime of a seal [3, 4].

Strain energy is the energy that is absorbed by a material as a result of deformation from an applied external load or stress. For a uniaxial loading case, the strain energy is simply the area under the stress-strain response curve. To eliminate size as a factor, the strain energy per unit volume, or the strain energy density, *u*, is considered. For a general stress loading case, from [5], elastic strain energy density, *u*, is defined as the strain energy per a unit volume,

$$u = \frac{1}{2}(\sigma_{xx}\varepsilon_{xx} + \sigma_{yy}\varepsilon_{yy} + \sigma_{zz}\varepsilon_{zz} + \tau_{xy}\gamma_{xy} + \tau_{yz}\gamma_{yz} + \tau_{zx}\gamma_{zx}).$$

2.2. Literature Review

Over time, a variety of work has been conducted in order to try to model the behavior of elastomer materials for sealing applications. There have also been considerable efforts dedicated to the measurement and prediction of compression set properties of seals, but the inability to accurately predict compression set is an important and challenging problem.

In 1990, Bower and Ledbetter [7] developed an analytical and numerical procedure for the prediction of compression set resulting from small strains at relatively short times using material property data, with the assumptions that the material is homogeneous, isotropic, and linear viscoelastic. Experimental stress response data used in their approach was approximated to be linear. The approach was limited because compression set predictions inconsistently fell within agreement to experimentally measured compression set values for a small range of testing temperatures, and for short periods after load removal from o-ring.

Additional limitations included the assumption that the o-ring was made of a single homogeneous material.

In 1988, Dragonni and Strozzi [8] experimentally and numerically analyzed stress fields in o-rings that sat in and were laterally restrained by a rectangular groove. Modeling accounted for lateral restraining effects for compressions below 15%. They found that laterally restrained o-rings do not suffer from appreciable tensile stresses at the center of the seal cross-section. Therefore, the plane-strain analysis method is valid for describing the stress-strain field if the ratio between toroidal seal diameter and cross-section diameter is sufficiently high (≥5).

Recognizing the need to fully understand the static properties of seals before proceeding to accurately modeling dynamic behavior, in 1992, Green and English [9] investigated the static stiffness characteristics of hyperelastic o-rings using commercially available finite element analysis (FEA) software. Their models showed that varying Poisson's ratio from 0.490 to 0.495 had a negligible effect on the calculated stress states across seal cross-sections. Models were run with Poisson's ratios up to 0.4999 without any code locking, or singularities. The results also validated the plane-strain assumption in o-ring analysis using hyperelastic material models.

In 1997, Warren and Weese [10] investigated the effects of a three-dimensional state of stress in the compression of seals between smooth, frictionless rigid plates. They noted the importance of considering the effects of toroidal radius expansion during o-ring compression. Due to the near-incompressible properties of elastomers, under certain conditions, this radial expansion can significantly decrease the cross-sectional o-ring area and contact area between the seal and glands, resulting in a lower seal-gland contact pressure. If unaccounted for, this can compromise sealing integrity.

In 2001, Akisanya et al. [11] examined how an appropriate use of material in seal design can help to minimize the risk of one of the major causes of failure in packing elements. The outer region of the cylindrical packing element was made of a fiber-reinforced elastomer. Numerical results showed that appropriate material combinations in the design and

manufacture of sealing elements led to significantly less seal extrusion, a major failure mode in the packing elements, and thus their designs avoided the need of mechanical anti-extrusion devices, and demonstrated the usefulness of varying material behavior over the cross-section of a seal.

A major problem with interpreting compression set measurements is the fact that measured values depend largely on the elapsed time between load removal and post-strain measurements. In 2004, Gillen et al. [12, 13] investigated the relationship between sealing force and compression set, and formulated a failure criterion for sealing force – i.e. the force at which leakage occurs. They developed methods of oven tempering and over-straining experimental o-ring samples to determine the long-term behavior and compression set measurements of different o-ring materials. The aims were 1) to predict equilibrium values of permanent deformation, i.e. the point where the growth of permanent deformation becomes negligible, and 2) eliminate the variance of compression set measurements that occur with the amount of time elapsed between load removal, and measurements. Field compression set data from o-rings in use up to 25-years were correlated reasonably well to extrapolated data from elevated temperature aged o-ring samples. Linear relationships between sealing force and compression set were also determined that allow a reasonable approximation of sealing force based on compression set measurements. The methodology was material dependent and the data had a fair degree of scatter.

In 2005, Bigg et al. [14] demonstrated that perfluorinated polyether rubbers displayed an appreciable degree of retained sealing force in o-rings during compression stress relaxation tests. Compression set values of the perfluorinated rubber specimens were considerably lower than those of nitrile rubber specimens. Their work indicated the importance of appropriate material selection for seal design.

Permanent deformation in elastomers is due to the occurrence of both chain scission and cross-linking reactions. In 1946, Andrews et al. [15] developed a method of quantitatively describing the permanent set taking place in vulcanized natural and synthetic rubbers under constant strain at elevated temperatures. In 2000, Bergström and Boyce [16] attempted to model the rate-dependent response of elastomeric materials by isolating the

time-dependent and long-term equilibrium response components. They suggested that the material can be modeled by two polymer networks acting in parallel: the first, an equilibrium state "perfect network" that can be modeled by classic hyperelastic models, and the second, a time-dependent element in series with the "perfect network" which aims to capture the material behaviors observed in experimental investigations. They conducted experiments on a series of filled chloroprene and natural rubbers and documented the effects of filler particle volume on stress and strain responses. The proposed model agreed with experimental data for both materials and showed that it is possible to predict the behavior of elastomers for different strain rates, and loading and unloading cycles.

In 2000, Achenbach [17] developed a service life prediction technique based on the chemical deterioration rates and the strain energy concept. A strain energy function was proposed which described the elastic properties of rubbers with the ability to consider long term and temperature effects. The strain energy function is a scalar function that relates the strain energy density to a deformation gradient. The initial strain energy function, at time t=0, was designed so that the state of zero deformation was the lowest point (point of minimum energy) and corresponded to a local minimum on the curve. After the application of a load, the approach was to lower, or "rotate", the strain energy function with respect to time. This curve rotation represented the effect of long-term deformation. See Figure 4. The function eventually reached a lower limit where stress relaxation no longer occurred. Through this approach, once the load was removed from a material, the new strain energy function allowed the determination of the new point of minimum energy, i.e. the lowest point on the curve, and this local minimum represented the amount of permanent deformation.

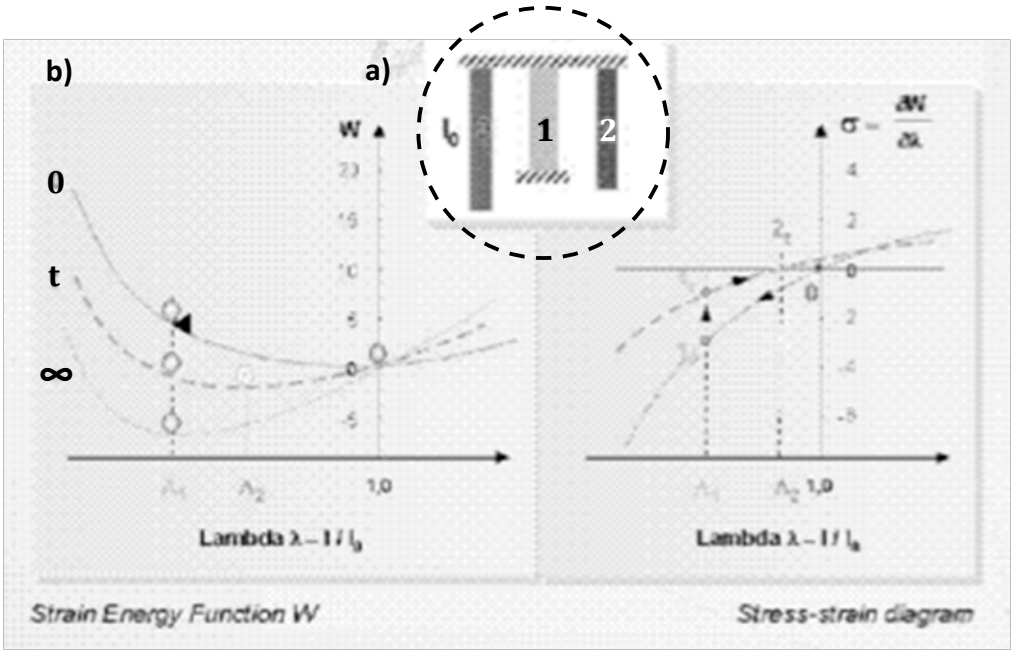

Figure 4: Changing Strain Energy Function
Strain energy function proposed by Achenbach [17]. 4a demonstrates a material at an initial state, I_o, that is compressed to State 1, and released, rebounding to its new shape shown in State 2. 4b demonstrates the evolution of the strain energy density function at a time, t = 0, before the application of a load, and t = ∞, where permanent deformation ceases.

In 1991, Nilkanth and Campbell [18] showed in their work that FEA simulation could give accurate information regarding installation force, deformation patterns under compression, and stress distribution within the seal cross-section when an accurate material model is used. An accurate model takes into account the material response to different modes of strain (e.g. compressive, tensile, and shearing loads.) They studied both static and dynamic sealing applications and emphasized the importance of the accuracy of nonlinear material models. Experimental methods used to determine material behavior and material models must be representative of the application conditions. For example, elastomer compounds respond differently to compressive and tensile loads due to their near incompressible nature. In its compressed state, the material in an o-ring cross-section is in compression near the seal-gland interface, but is actually in tension near the free edges. Therefore, at the very least, both of these properties are needed in the material model in order to accurately simulate o-ring behavior.

In their FEA models used to design an elastomeric seal, Calvert et al. [19] designed a test rig and conducted experiments to obtain friction data between the seal-gland interface, and found average friction coefficient values, μ, of 0.24 to 0.26 at room temperature.

2.3. Related Work

In 2007, Sefkow [3] and Maciejewski [4] developed design principles to decrease the effects of compression set in o-rings. After defining a measure of performance that depended on compression set, photoelastic analyses on essentially two-dimensional disk-shaped polyurethane specimens were used to verify the accuracy of numerical models of circular o-ring cross-sections. The numerical models were then used to further study the effects of material properties and material distribution on the state of stress in o-ring cross sections.

The development of the seal design concept was based on experimental results similar to those shown in Figure 5. Two types of tests were conducted to demonstrate the compression set phenomenon. In one set of experiments, cylindrical polyurethane specimens were wrapped and compressed by varying amounts. Specimens were held in the compressed state for varying lengths of time, unwrapped, and compression set measured. In a second set of experiments, the load-deflection behavior of compressed cylindrical specimens was measured at various times. The load needed to produce a 20% diametric compression was used to characterize material behavior as a function of time. The results were characterized in several ways, including describing them in terms of strain energy density. The strain energy density was calculated for all specimens and is shown in Figure 5 along with compression set and the load deflection behavior characterization. The correlation between strain energy content and permanent deformation led to selecting strain energy as a seal design variable.

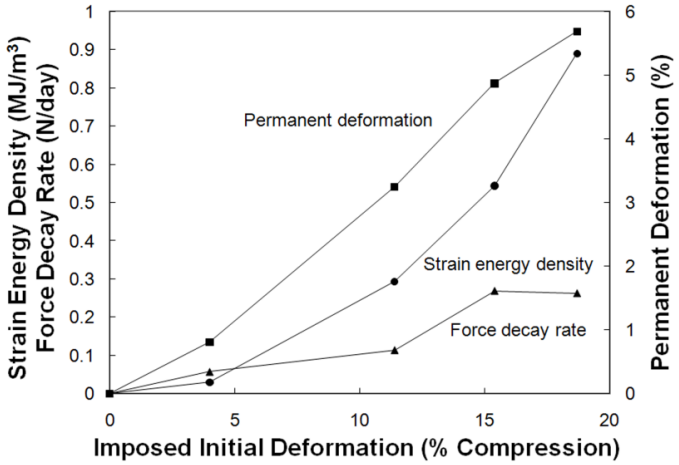

Figure 5: Strain Energy, Permanent Deformation, and Imposed Initial Deformation
Strains imposed on cylindrical elastomer samples showed the correlation between increasing permanent deformation and increasing strain energy density. Sefkow et al. [20].

In the work by Sefkow [3], photoelastic analysis was conducted on two-dimensional o-ring cross-sections that showed that the stress-strain field and strain energy density field vary considerably over the seal cross-section. Typical results are shown in Figure 6. The region of highest strain energy was shown to be located near and below the seal-gland interface. Modified sections were produced that contained an inset region of a different material behavior near the upper and lower boundaries of the cross-section. These results led to the concept of controlling strain energy by modifying material behavior in high-energy regions in a seal cross-section. Experimental results were used to validate FEA models used in subsequent design studies where inset regions were included with various material stiffness values, sizes, shapes, and locations, to determine the effects on strain energy density distribution.

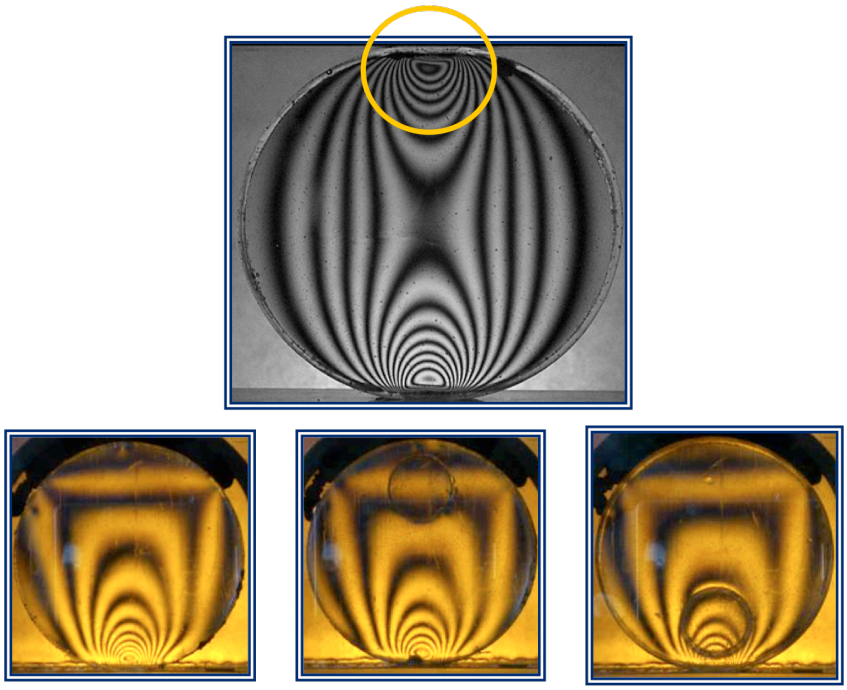

Figure 6: Photoelastic Studies of O-ring Cross-Sections
Photoelastic studies show regions of high stress in o-ring cross-section, and were used to validate numerical studies [20].

The work of Sefkow and Maciejewski yielded three important results that are the starting point for this work. First, results demonstrated that insets of varying elastic moduli placed in regions of high ESED changed the patterns and stress gradients across the o-ring cross-section. Second, o-ring inset sections of a less-stiff material led to decreased overall strain energy levels in the seal sections. Third, time-dependent simulations showed that the rate of stress relaxation decreases as ESED is lowered over the seal cross section. These concepts were used throughout this work, and following is an overview of all the research done to address the problem of improved seal design based on minimizing strain energy in the seal.

3. Overview of Research

3.1. Motivation

Even in optimal operating environments, the performance of elastomeric seals will degrade over time due to the onset and growth of permanent deformation as described in Section 2. The loss of sealing pressure and leakage of working fluids can have severe consequences on system effectiveness and in some applications can also lead to environmental concerns. Being comprised of many wearable items, including critical sealing components, many fluid power systems require periodic preventive maintenance, and encounter problems due to seal failure, which results in machine downtime, service costs, and repair costs. Extending the lifetime of seals will reduce maintenance intervals and unexpected equipment downtime, resulting in increased equipment productivity and cost savings.

3.2. Specific Goals

This research aimed to determine modes of utilizing material behavior that result in improved long-term seal performance. The focus was two-fold. The first focus was to determine seal designs that demonstrate a decrease in rates of stress relaxation while under compression. These seal designs were the basis for the second focus, which was to determine modes of utilizing material behavior to increase the maximum potential sealing pressure of these new seal designs. The specific goals of this work were to:

- Determine the effect that varying material properties across an o-ring seal cross-section have on the resulting strain energy content and maximum sealing pressure.
- Create experimental o-ring seals demonstrating the design concept.
- Measure permanent deformation in o-ring designs through compression set tests.
- Measure the performance of o-ring designs over time by compression stress relaxation tests.

- Increase maximum potential contact pressure by determining the effect that strain-stiffening material behaviors incorporated into o-ring designs have on the resulting strain energy content and maximum sealing pressure.
- Demonstrate retained sealing pressure over time with the use of materials that exhibit adaptive-stiffening behavior.

3.3. Research Approach and Overview of Methods

Material behavior and its application to seal design is the main concentration of this work. Since this is a new approach to seal design, analytical methods, numerical modeling, and experimental work focus on o-rings in static settings. The o-ring seal was chosen in this investigation because of its widespread use and applicability. Its simple geometry allowed for less complex analytical and numerical techniques to be used in the research. Also, the simple geometry allowed the production of experimental o-rings by casting using an easily constructed molding apparatus. Additionally, thermal and chemical processes that can have significant effects in particularly severe environments were not considered in this work. All material models were isotropic and material friction coefficients were taken into consideration at the seal-gland interface using values determined in previous work [19]. It is expected that design rules developed for o-ring seals through this research can be expanded to different seal geometries, dynamic applications, and applications where other ambient factors can be considered.

3.3.1. Strain Energy Content and Sealing Pressure

The starting point of this work was to develop a numerical model to identify material behaviors and o-ring designs that resulted in lower strain energy levels across the seal cross-section when compared to a baseline o-ring. Hertz's contact stress equations show that the maximum stress and strain in a static elastic circular body in contact with a static flat body occurs just below the contact interface [3]. Since strain energy is highest where stress and strain are both high, this region is also the area of maximum strain energy density. In order to minimize this region of high strain energy, the stress and/or strain needs to be lowered. A major challenge in this work was modifying the stress and strain fields in the o-ring cross section in such a way that the resulting strain energy density was

quantitatively lower, while still allowing the seal to maintain an adequate contact pressure with the gland.

As suggested by the work of Sefkow and Maciejewski [3, 4], to reduce the amount of strain energy content in the seal, the elastic modulus, *E*, of the region in the o-ring that experiences the highest ESED is decreased. Throughout the work, these regions of modified material properties within the seal are referred to as insets. Since the static compression of the o-ring remains the same for all o-ring designs, i.e. the seal experiences the same state of strain, this inset of modified material properties causes the resulting stress to decrease because stress is directly proportional to strain by the constant, *E*. Therefore, as the elastic modulus decreases, so will the stress.

Inset stiffness and placement were varied in numerical studies to gather data that would lead to identifying the ideal regions where material property modifications can have the greatest effect on overall seal performance. Methods and results are detailed in Section 4.

3.3.2. Demonstration of Concepts with Experimental O-rings

In order to demonstrate the usefulness of the design concept beyond numerical simulations, experimental o-ring samples were manufactured from a commercially available molding rubber compound. Modified material properties across the o-ring cross-section were realized by including insets made of rubber materials that were softer than the main o-ring material. O-ring properties were characterized by hardness measurements. O-ring performance was measured in experiments where 1) permanent deformation was quantified through compression set measurements, and 2) long-term performance was quantified by observing compression stress relaxation, i.e. the rate of loss of sealing force over time. Experimental methods and results are presented in Section 5.

3.3.3. Increasing Sealing Pressure

Previous numerical simulations as well as limited experimental results demonstrated improved seal performance in terms of a decreased rate of contact pressure loss. However, this improved retention rate of sealing pressure was accompanied by a decrease in the initial sealing pressures of the seal designs. That is, new seal designs demonstrated less

maximum sealing pressures when compared to baseline designs. To address this issue, two additional investigations were undertaken in this work.

Since changing the properties of materials over the seal cross-section proved beneficial to seal design, this suggested that even more extreme material behavior modifications could prove useful. First, the natural strain-stiffening behavior of many elastomer materials exhibited at high strains is manipulated to be evident at fairly low strains encountered in standard sealing applications. Also, most elastomer materials respond differently to the type of loading being encountered, e.g. uniaxial, equibiaxial, or shear loads. These behavioral responses were isolated and modified in design studies. The approach was to determine material behaviors that could be incorporated into seal designs that would result in decreased strain energy content in the seal, while maintaining higher sealing pressure levels than those from previous results. Numerical simulations were performed, and the results are presented in Section 6.

3.3.4. Maintaining Sealing Pressure Over Time

The benefit of minimizing strain energy as a useful parameter in seal design has been emphasized. However, the viscoelastic properties of elastomer materials lead to a decrease in strain energy content stored in a seal over time. This is evident by the compression stress relaxation phenomenon described earlier. Upon initial o-ring compression, a seal with low strain energy when compared to a baseline design is desired. However, a decrease in this strain energy over time is not desired, as it compromises the ability of the o-ring to perform its sealing function.

Material models were created that increase in stiffness over time, and these materials were incorporated into new o-ring designs as insets. As in the work to be described in Sections 4 and 6, this behavior is confined to the high strain energy regions of the seal under compression. Section 7 describes the numerical methods used, and presents results that demonstrate the ability of o-ring designs utilizing this material to better maintain sealing pressure over time compared to a baseline o-ring design.

4. Numerical Simulations – Linear Materials

Numerical simulations were conducted in a finite element package to determine the distribution of elastic strain energy density (ESED) and the resulting maximum sealing pressure for different o-ring designs under a static loading. Numerical simulations have been validated in many different past studies. [3, 4, 7, 8, 10, 15, 17]. The goals of these numerical studies were to 1) demonstrate the effect of material properties on ESED distribution, 2) demonstrate the effect of inset placement on the resulting maximum potential sealing pressure for the seal design, and 3) gain an understanding of inset placement on these quantities for applications to further studies.

To begin, design parameters were assembled in order to create baseline data that described how ESED and seal-gland contact pressure would vary with the elastic modulus, E, and the placement of insets in different o-ring configurations. With the goal in mind of eventually creating experimental o-ring seals, industrial seal catalogs [1] were reviewed in order to determine applicable dimensions for the numerical models.

4.1. Describing Materials

Material stiffness was one of the parameters used to create different o-ring designs for the numerical simulations. While there is no direct correlation between elastomer modulus of elasticity and hardness measurements, stiffness empirically increases with an increase in measured hardness. A relationship identified by Hertz Jr. [21] for common industrial rubber o-ring seals was used to determine the approximate stiffness values for varying hardness values, so that the stiffness values used would be relevant to real o-ring seals. The elastic modulus vs. hardness data was plotted, and a fifth-order polynomial was fit to the data for use in extrapolating hardness values outside the range of values from that study. Figure 7 presents the relationship established by Hertz Jr. In Table 1 the elastic modulus values used in this work are shown with their corresponding hardness values.

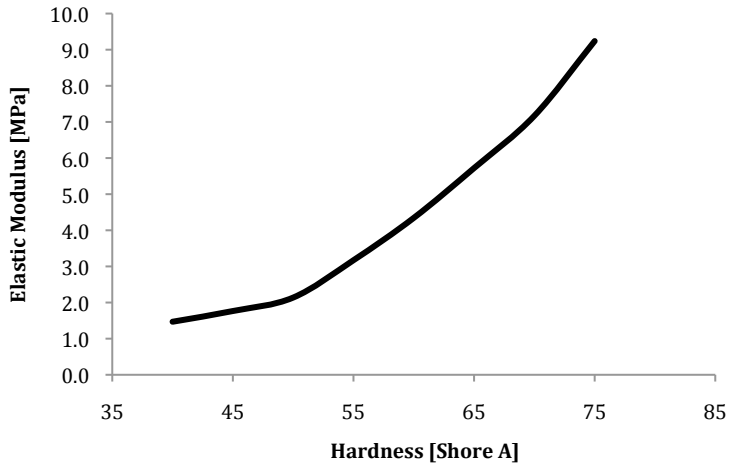

Figure 7: Elastic Modulus vs. Hardness
Hertz Jr. [21]

Table 1: Material Properties for Linear Material Models

Material	*Hardness [Shore A]*	*Stiffness [MPa]*	*Material*	*Hardness [Shore A]*	*Stiffness [MPa]*
A	80	13.4	F	67.5	6.4
B	77.5	10.9	G	65	5.7
C	75	9.2	H	62.5	5.1
D	72.5	8.1	I	60	4.4
E	70	7.2	J	57.5	3.7

Elastic modulus values, *E*, used in numerical simulations. The letters A through J are a labeling scheme, and do not represent any physical material properties.

4.2. Numerical Simulations

4.2.1. Numerical Model Development

An axisymmetric model was set up in a commercial FEA software package. A large deformation analysis was conducted, which accounts for the nonlinearity introduced by the changing shape of the deformed elements as the overall geometry changes [25]. The o-ring was 8.4-mm in diameter, and had an inner diameter of 144.5-mm. The o-ring cross-section was meshed with 28642 quad plane elements. The glands were represented by a very rigid material with an elastic modulus of 210-GPa, and a Poisson's ratio of 0.3. Two contact pairs were created: one at the upper and one at the lower seal-gland interface. The o-ring surface was assigned 464 contact elements and the upper and lower glands were

represented by rigid line target elements. A coefficient of friction of 0.24 was used in the analysis [19]. A Poisson's ratio of 0.495 was used for all materials in these simulations.

An o-ring made of a single homogeneous material with an elastic modulus of 13.4-MPa was studied in order to determine the baseline behavior for comparison to o-ring designs with different material properties. The o-ring was compressed 15% of its diameter, and Figure 8 shows the strain energy density distribution and contact pressure profile. The elastic strain energy density has an hourglass like distribution for the regions with higher stress levels. The yellow region represents the highest strain energy density values, ranging from 0.307 to 0.359-MJ/m^3. The contact pressure profile is parabolic, and the red region represents the highest values. The maximum contact pressure of 3.83-MPa occurs at the center of the contact area of the upper and lower glands because of symmetry.

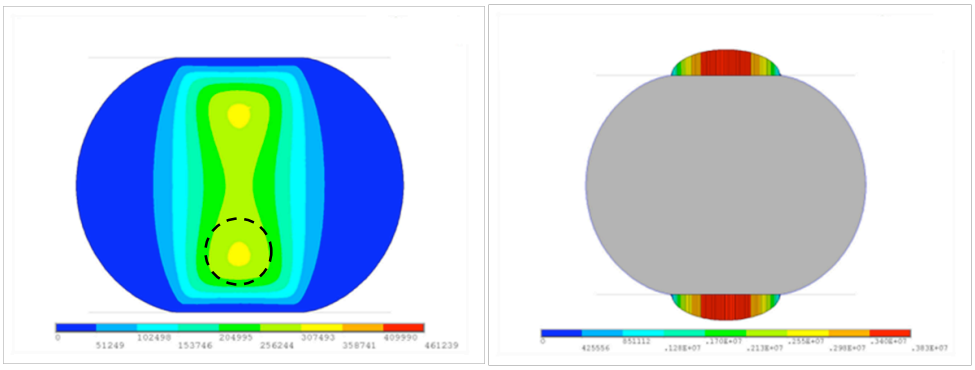

Figure 8: ESED Distribution and Contact Pressure Profile for Baseline O-ring
A one-material o-ring of E = 13.4-MPa under a static 15% compression. Left: ESED distribution – yellow represents the highest energy values, and blue the lowest values. Right: Contact pressure profile, with red contours representing highest values.

The numerical studies that followed investigated o-ring sections with insets of softer materials. Inset stiffness and inset location were varied. Two primary inset locations were chosen for comparison. The first was chosen to cover the region of highest ESED, as indicated in the dashed enclosed region in Figure 8. Since this region is approximately circular in shape, the approximate center of the location was determined, and this location was chosen as the initial location for the placement of a material inset with different properties. This location was located at a pre-compression point vertically offset d_o = 2.065-mm from the main o-ring center. The second inset location was just below the seal-gland

interface. Inset placement for both cases is shown in Figure 9. The inset diameter for both o-ring designs was 1.8-mm.

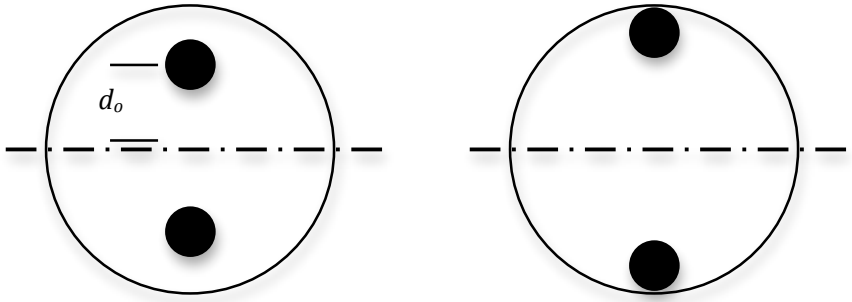

Figure 9: Inset Placement for Linear Material Numerical Simulations

To impose a load on the o-ring, the bottom gland was fixed to have no vertical or horizontal movement, and the top gland was assigned a purely vertical movement of 1.26-mm to simulate the closing of the o-ring gland compressing the o-ring by 15% of its diameter. The simulations were time-independent. All values resulting from the simulations used in data analysis were at the maximum compression.

4.2.2. Results

The two main mechanical quantities chosen for characterizing seal behavior were generated ESED and contact pressure. The FEA software calculates ESED as,

$$ESED = u = \int \vec{\sigma} \cdot d\vec{\varepsilon}_{el} = \sum \frac{1}{2}(\sigma_1 + \sigma_2) d\varepsilon_{el},$$

where ε_{el} is the elastic strain.

The results of the design studies showed that some o-ring designs would contain very small regions of very high ESED values. In order to quantify the entire strain energy content in the seal for direct comparison between different o-ring designs, a dimensionless value, *ESED intensity*, was computed from ESED contour plots, e.g. as shown in Figure 8. Contour plots were generated using the finite element package, and the contours represented nine different ranges of values: blue – a value of zero, to red – the highest ESED value. Each color represented equal ranges of ESED values.

After all simulations were completed, all the results were reviewed to determine which design contained the highest ESED value, $ESED_{max}$. The range of values for the ESED contour plot of each o-ring design was adjusted to capture all strain energy values from 0 to $ESED_{max}$. Imaging software was used to count the number of pixels in each contour color, which is defined as Π_i, where i ranges from 1 to 9, and i = 1 represents the contour color with the lowest ESED values, and i = 9 represents the contour color with the highest ESED values. The total number of pixels in the entire contour plot is defined by Π_T. *ESED intensity* was define as,

$$\sum_{i=1}^{9} \frac{100 \cdot (i \cdot \Pi_i)}{\Pi_T}.$$

Sample imaging analysis data, and a demonstration of the calculation of ESED intensity for one group of o-ring designs with the inset offset from the surface, are presented in Table 2 and Table 3. The maximum ESED intensity seen in all cases was 2.619 for the baseline design made of one material with a stiffness of 13.4-MPa. The maximum sealing pressure of 3.83-MPa was also seen in the baseline design. Maximum contact pressure results are presented in Table 4. All values presented in Table 3 and Table 4 were normalized by the maximum values seen in the baseline design.

Table 2: Sample Imaging Analysis Data

Design	*Contours*	*High* $i = 9$	$i = 8$	$i = 7$	*Middle* $i = 6$	$i = 5$	$i = 4$	$i = 3$	$i = 2$	*Low* $i = 1$
Main - Inset	ESED [MJ/m³]	0.410 - 0.461	0.359 - 0.410	0.305 - 0.359	0.256 - 0.308	0.205 - 0.256	0.154 - 0.205	0.103 - 0.154	0.0512 - 0.103	0 - 0.0512
A	Pixels, Πi	0	0	7062	63532	56284	51921	54755	69290	265212
	% of total	0.0%	0.0%	1.24%	11.18%	9.91%	9.14%	9.64%	12.20%	46.69%
A - B	Pixels, Πi	0	0	0	40555	75629	58547	56074	69999	266752
	% of total	0.0%	0.0%	0.0%	7.1%	13.3%	10.3%	9.9%	12.3%	47.0%
A - C	Pixels, Πi	0	0	630	18784	79457	74063	56233	70552	268064
	% of total	0.0%	0.0%	0.1%	3.3%	14.0%	13.0%	9.9%	12.4%	47.2%
A - D	Pixels, Πi	0	0	1019	4429	73452	93133	57087	70830	269232
	% of total	0.0%	0.0%	0.2%	0.8%	12.9%	16.4%	10.0%	12.4%	47.3%
A - E	Pixels, Πi	0	0	1338	4034	58733	106458	58346	70952	270188
	% of total	0.0%	0.0%	0.2%	0.7%	10.3%	18.7%	10.2%	12.4%	47.4%
A - F	Pixels, Πi	0	15	1477	3601	38418	125022	59544	70915	271052
	% of total	0.0%	0.0%	0.3%	0.6%	6.7%	21.9%	10.4%	12.4%	47.5%
A - G	Pixels, Πi	0	173	1641	3581	16720	142858	60568	70906	271852
	% of total	0.0%	0.0%	0.3%	0.6%	2.9%	25.1%	10.7%	12.5%	47.8%
A - H	Pixels, Πi	0	289	2007	3046	15710	134282	64387	71041	272848
	% of total	0.0%	0.1%	0.4%	0.5%	2.8%	23.8%	11.4%	12.6%	48.4%

Table 3: Sample ESED Intensity Calculation

O-ring Design Main - Inset	*Pixel Total,* Π_T	*Deviation from Average*	*ESED Intensity*	*Normalized Intensity*
A	568056	0.15%	2.619	1.00
A - B	567556	0.07%	2.521	0.96
A - C	567783	0.11%	2.446	0.93
A - D	569182	0.35%	2.382	0.91
A - E	570049	0.51%	2.351	0.90
A - F	570044	0.51%	2.308	0.88
A - G	568299	0.20%	2.261	0.86
A - H	563610	-0.63%	2.233	0.85

Table 4: Maximum Contact Pressure

	Inset Offset from Surface		*Inset at O-ring Surface*	
O-ring Design Main - Inset	*CP_{max} [MPa]*	*Normalized CP*	*CP_{max} [MPa]*	*Normalized CP*
A	3.83	1.00	3.83	1.000
A - B	3.54	0.92	3.46	0.903
A - C	3.32	0.87	3.23	0.843
A - D	3.15	0.82	3.21	0.838
A - E	3.02	0.79	3.21	0.838
A - F	2.92	0.76	3.22	0.841
A - G	2.83	0.74	3.23	0.843
A - H	2.75	0.72	3.25	0.849
A - I	-	-	3.26	0.851
A - J	-	-	3.28	0.856

Normalized ESED intensity and maximum contact pressure values are shown in Figure 10. The left-most data points represent ESED intensity and contact pressure of a one-material baseline design with a modulus of elasticity of 13.4-MPa. The remaining data points represent ESED intensity and contact pressure for designs that include insets made of softer materials. The stiffness of the inset region decreases in the samples moving from left to right.

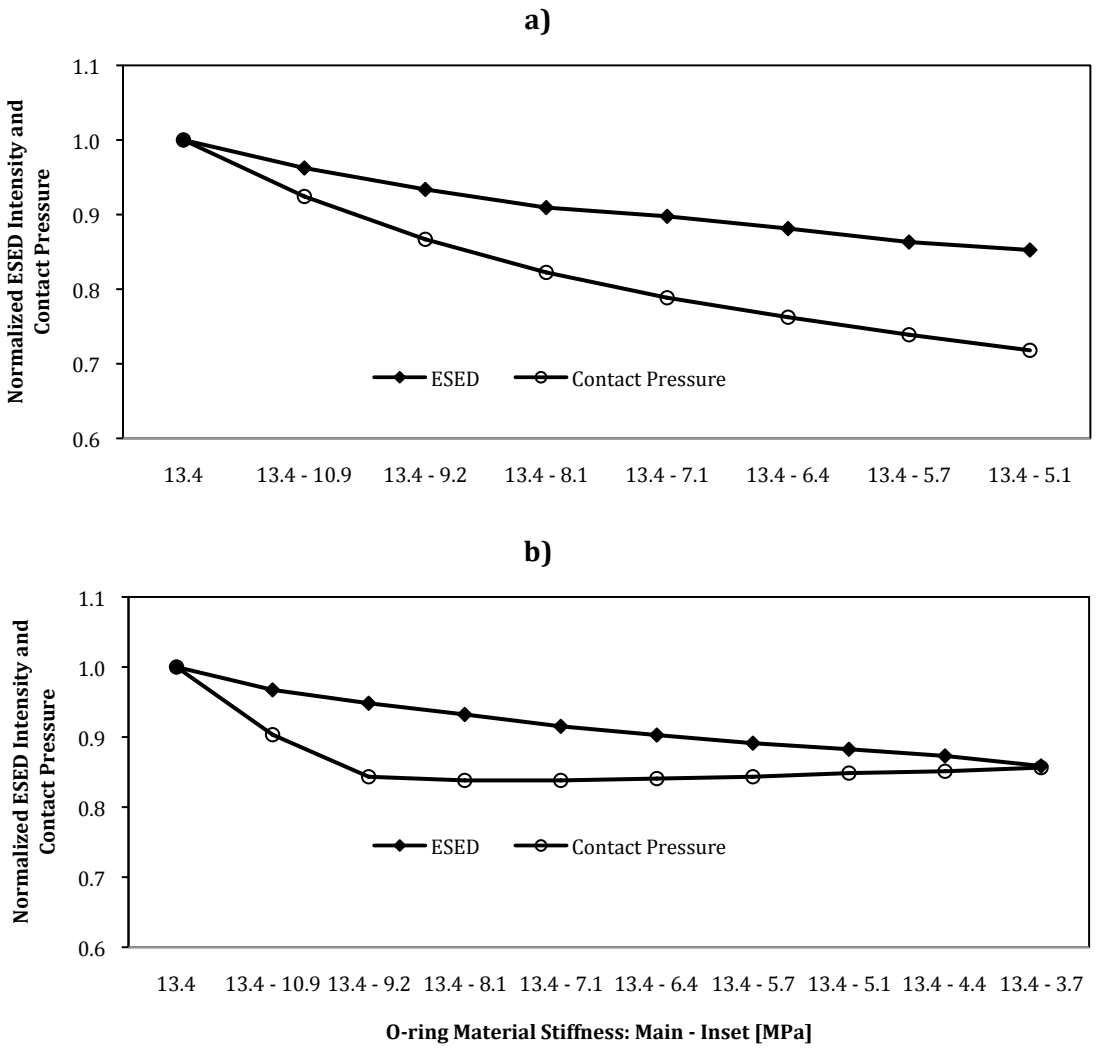

Figure 10: Linear Material Models – Numerical Simulation Results

ESED intensity and maximum contact pressure both normalized on a scale from 0.0 to 1.0 for a) an o-ring design with the inset offset 2.065-mm from the center of the o-ring and b) an o-ring with the inset just below the surface.

Figure 10a presents the results for an o-ring with the inset material region offset 2.065-mm from the center of the o-ring to directly cover the region of highest strain energy. The results show that as the stiffness of the inset is decreased from 10.9-MPa to 5.1-MPa, normalized ESED intensity decreases from 1.00 for the baseline design, to 0.85 for the o-ring with the 5.1-MPa inset, a decrease of 15%. It is also observed that the normalized maximum contact pressure decreases an even larger amount for the same o-ring designs, from 1.00 to 0.72, a decrease of 28%.

When the inset is placed right at the o-ring surface, the loss of sealing pressure can be mitigated while maintaining lower strain energy content across the seal. Figure 10b shows that as the difference between stiffness of the main o-ring section and the softer inset is increased, the decrease in contact pressure is initially severe slows as the stiffness of the inset is decreased further. As the inset stiffness is decreased from 10.9-MPa to 5.1-MPa, the ESED intensity consistently decreases from 1.00 for the baseline design, to 0.88, a decrease of 12%. However, for this inset configuration, the maximum contact pressure for the o-ring is higher than the previous design with insets of the same stiffness placed at a different location. Here, as the inset stiffness decreases to 5.1-MPa, the normalized maximum contact pressure decreases from 1.00 for the baseline design, to 0.85-MPa, a decrease of only 15%.

It is also interesting to note that in contrast to the constant decreasing contact pressure pattern observed in the previous o-ring design, when the inset is near the o-ring/gland surface, and significantly less stiff that the surrounding o-ring material, the maximum contact pressure begins to increase again slightly. The lowest normalized contact pressure of 0.84 was for the design that had an inset of 9.2-MPa. As the stiffness of the inset is lowered to 3.7-MPa, the contact pressure creeps back up slightly to a value of 0.86.

The inference from comparing the two different o-ring designs is that inset location is an important design parameter when the inset region is much less stiff than the surrounding material. In these designs, the larger o-ring section has a more dominant role in determining the overall maximum sealing pressure of the seal. These results make evident the ability to control both seal strain energy content and maximum potential sealing pressure by modifying material behavior and the distribution of material behavior.

The design studies summarized show that an o-ring including an inset made of a softer material allows the seal to experience less strain energy the seal cross-sections. However, all designs also produced a decreased maximum contact pressure. Therefore focus was placed on identifying and modeling material behavior that could serve to recuperate this lost contact pressure, while keeping a low ESED. Methods addressing this focus of the research are presented in Section 6 and Section 7.

5. Experimental Methods and Results

Several different o-ring designs from the numerical studies presented in Section 4 and previous studies [3, 4] exhibited decreased strain energy content across the o-ring cross-section, but no work had been performed to create and test real seals to obtain experimental data to validate these simulation results. The goal of the experimental work was to 1) create real experimental o-rings that implemented designs evaluated numerically in previous work, 2) design and perform compression stress relaxation tests, 3) design and perform compression set tests, and 4) validate the seal design concept with experimental data.

5.1. Creating Experimental O-ring Samples

As part of this work, o-ring samples were created with an industrial rubber molding compound, Flexane® 80 Liquid, manufactured by Devcon® [Appendix B]. This compound was chosen because of its maximum potential hardness, the ability to vary the resulting hardness, its operating temperature range, and indicated use in other industrial applications. The approach was to use the Flexane material as the main o-ring material and include insets made of a softer rubber material to determine the effect on permanent deformation.

5.1.1. Material Behavior: Tensile Tests

Before creating o-ring samples, tensile samples were cast with specifications recommended by ASTM D412 [22] guidelines. These samples were created to verify that the cured Flexane compound would display appropriate viscoelastic behavior before proceeding to use the material for the o-ring test samples. Samples were cast from three different mixing ratios of the resin, casting agent, and optional softening agent. The different mixing ratios yielded a cured rubber with varying stiffness and Shore A hardness properties. This data is presented in Table 5. The hardness specifications listed were the predicted results based on the manufacturer's recommended mixing ratios.

Table 5: Approximate Material Hardness for Different Mixing Ratios

Specimen	*Predicted Hardness [Shore A]*	*Resin [%]*	*Casting Agent [%]*	*Flexibilizer [%]*
A	87	77	23	0
B	78	70.24	20.98	8.78
C	72	59.96	14.99	17.91

Tensile tests were conducted following ASTM 412 recommendations on a mechanical tensile test machine. The three different specimens were extended 15%, 7.6-mm, and held for 30-hours. As shown in Figure 11, all three specimens exhibited elastomeric behavior, i.e. viscoelastic behavior. A sharp initial loss of the resistance force was observed in the first couple hours of each specimen, and then the rate of force loss slowed. Specimen A exhibited a higher initial load than that of Specimen B, and similarly, Specimen B exhibited a higher initial load than that of Specimen C, as expected given the predicted hardness and stiffness properties of each specimen.

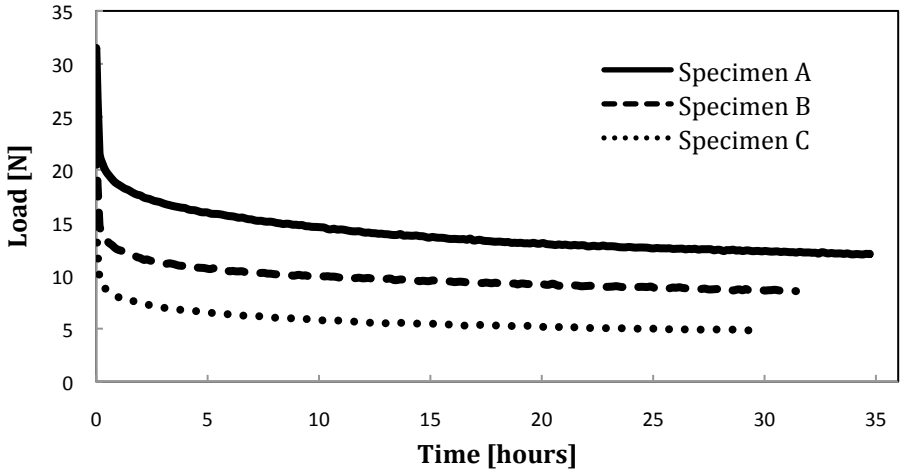

Figure 11: Flexane Material Tensile Tests

5.1.2. O-ring Design

After it was verified that the industrial rubber compound demonstrated viscoelastic behavior, the next step was to create o-ring seals that included insets of a softer material. In order to increase the homogeneity of the o-ring samples, and to simplify the manufacturing

process, real industrial o-rings were used as the insets. The Flexane rubber was used as the main material of the o-rings, and was cast around the rubber o-ring insets. See Figure 12.

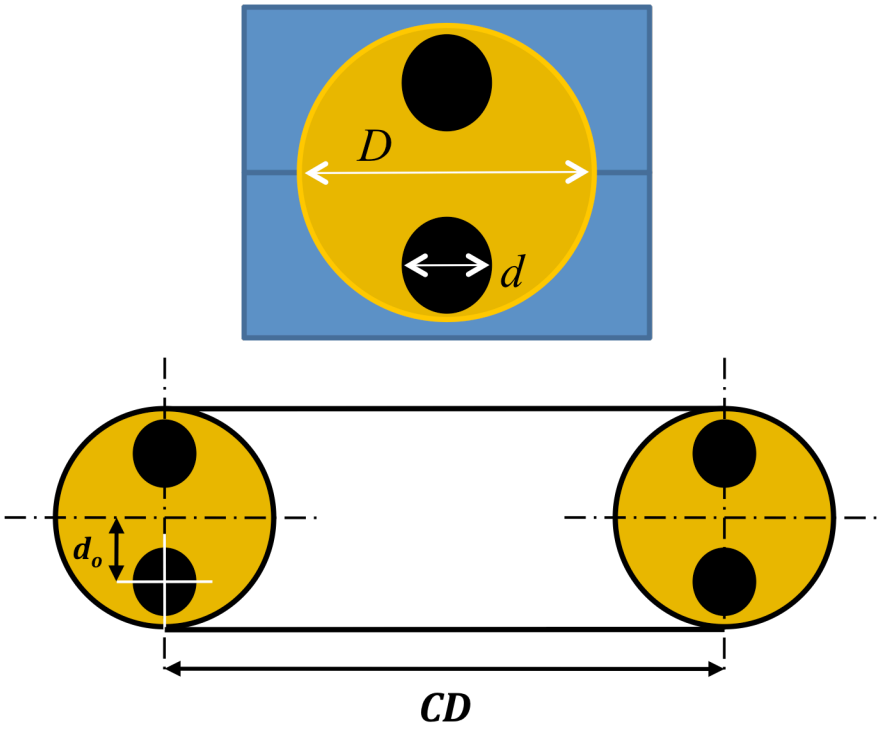

Figure 12: Experimental O-ring Schematic
Main o-ring made of Flexane material is shown in orange. Industrial o-ring seals acting as insets are shown in black. CD = 37-mm; D = 12.7-mm; d = 2-mm, 3-mm, and 4-mm; d_o was determined for each sample so the inset sat right at the o-ring edge.

Since numerical results showed that the size of the inset used has an effect on the ESED in the o-ring cross-section, the design variable for the experimental o-rings was the diameter of the inset. Industrial o-rings are typically catalogued by two specifications, 1) a cross-section diameter, and 2) the inner diameter of the o-ring torus. For this application of creating experimental seals, the goal was to find multiple o-rings that had a constant toroidal diameter, *CD*, to be used as potential insets so that the same o-ring mold could be use to make all o-ring samples. This was the main factor in determining the size of the main o-ring that could be cast.

Appropriate o-ring samples were located at a local seal supplier. Three o-rings with a *CD* dimension of 37-mm were found, with cross-section diameters of 2-mm, 3-mm, and 4-mm.

With these o-rings serving as the insets, the next step was to determine a way of molding an o-ring sample, with this same 37-mm toroidal diameter. Given the size of the insets, it was necessary that the main o-ring cross-section was large enough to accommodate two insets, while having the make-up of the entire o-ring be primarily of the Flexane material. An o-ring cross-section diameter of 12.7-mm was chosen due to tooling, specimen handling factors, and molding process considerations. O-ring specifications are listed in Table 6.

Table 6: Experimental O-ring Specifications

Design Designation	*O-ring Hardness [Shore A]*	*Inset Hardness [Shore A]*	*Inset Diameter, d [mm]*	*O-ring Diameter, D [mm]*	*CD [mm]*
Baseline	87	N/A	None	None	37
2-mm Inset	87	70	2	12.7	37
3-mm Inset	87	70	3	12.7	37
4-mm Inset	87	70	4	12.7	37

5.1.3. O-ring Mold

The Flexane material selected to create the o-ring samples cured at standard room temperature and pressure, which simplified the type of mold needed to cast the samples. Given the symmetry of the o-rings, the mold was designed to cast two o-ring halves. Experimenting with the compound showed that the pre-cured mixture was extremely viscous, and would allow the o-ring mold to be closed before a full cure, resulting in both o-ring-half volumes being joined without the need of additional adhesives. The mold halves were fabricated from aluminum plate. A ball-end end mill was used on a CNC milling machine to machine the grooves into the aluminum plates. Guiding pins were added to the mold structure to facilitate the alignment of the mold halves upon closing the mold. The o-ring mold is shown in Figure 13.

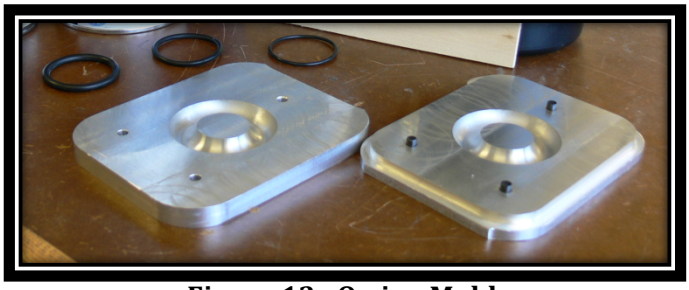

Figure 13: O-ring Mold
Mold halves used to create experimental o-ring samples.

5.1.4. Casting O-ring Samples

A standard operating procedure was created for the o-ring casting process, and is included in Appendix C. To begin, the mold halves were thoroughly cleaned to remove any oil, grease or dirt. A liquid release agent was applied to the mold to aid removal of the cured o-ring. Using the appropriate ratio of the casting agent and resin [Table 5] the compound was mixed according the manufacturer's specifications. Once mixed, a thin coating of mixture was spread around the mold. For the samples that required an inset, the inset was placed in the mold and centered at this time. The remainder of the mix was poured in a very thin stream to fill the mold cavity. A heating gun was used to blow hot air above the surface of the liquid form of the Flexane in order to smooth out the surface, and draw out any air bubbles forming in the mix. The material was allowed to rest for 30-minutes before closing the mold halves. After this 30-minute set, the mold halves were closed. A clamp was used to ensure a tight seal between the mold surfaces, and reduce the chances of leakage of the semi-viscous material. At this point, the closed mold was flipped every few minutes to assure that the sample would set evenly. The mold was allowed to cure for 10-hours before de-molding the samples. After de-molding, o-ring samples were allowed 7-days to reach a 100% cure according to manufacturer's recommendations. Figure 14 shows various stages of the o-ring mold casting process.

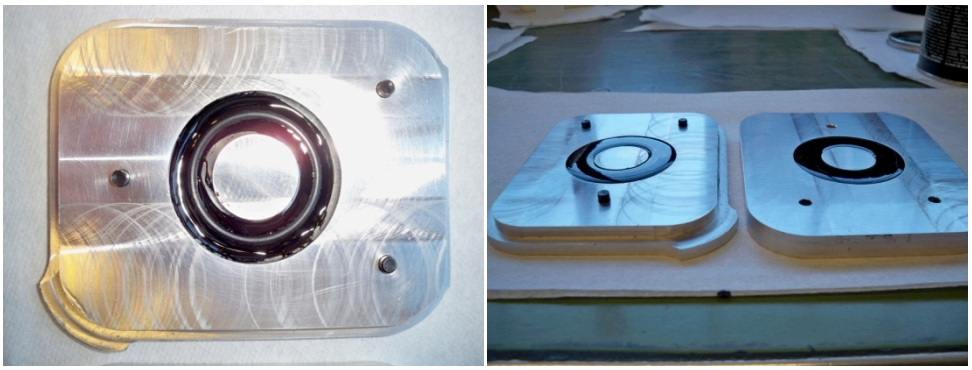

Figure 14: O-ring Casting Process
Left: O-ring inset placed on thin layer of elastomer mixture. Right: O-ring in the temporary set phase before closing mold and joining o-ring.

5.1.5. Hardness Testing of Samples

The mixing ratio of Sample A [Table 5] was used to mold four o-rings to test the hardness. After a few initial o-ring samples were cast, an IRHD Micro Compact II hardness tester was used to determine 1) how hardness ratings compared to those specified by the manufacturer, and 2) the consistency of the hardness throughout the cast o-ring sample. The IRHD Micro Compact II is specifically designed to determine the hardness of elastomer materials such as hoses, tubes, and o-rings. See Table 7 for technical details of the tester.

Table 7: IRHD Micro Compact II Technical Details

Test Method	*Total Force [mN]*	*Force on Foot [mN]*	*Indenter Ball Diameter [mm]*	*Measuring Distance [mm]*	*Range of Reading*
IRHD M	153.3	235	0.4	0.3	30-100

Similar to the Shore A hardness test, the IRHD test is based on measuring the penetration of a rigid ball-end indenter into a rubber specimen. The measured penetration is converted to a scale of degrees ranging from 0 to 100. A rating of 0 represents a material that has an elastic modulus of 0, and a reading of 100 represents a material that has an infinite elastic modulus. See ASTM D1415 [23] for full detail on the specified testing conditions. The elastomer testing literature shows that for highly elastic materials, the IRHD and Shore A scales are equivalent and comparable.

A top and bottom surface was indicated on each o-ring sample, and three testing points were identified on each surface, for a total of six testing points. The readings from these tests, presented in Table 8, show that the molded o-rings had an average IRHD rating of 91 degrees, with a good degree of consistency demonstrated by the small deviation values, the largest of which was 1.4 points. While the predicted Shore A hardness specified by Devcon for the Flexane compound was 87A, using the notion of the equivalence of both Shore A and IRHD scales, the IRHD rating is equivalent to a Shore A hardness of approximately 89. This falls within the tolerance of ±5 points on the Shore A scale.

Table 8: O-ring Specimen Hardness

O-ring Specimen	*Hardness 1st Point [IRHD]*	*Hardness 2nd Point [IRHD]*	*Hardness 3rd Point [IRHD]*	*Hardness 4th Point [IRHD]*	*Hardness 5th Point [IRHD]*	*Hardness Average [IRHD]*	*Standard Deviation*
1	92	92	90	-	-	**91**	**1.2**
2	91	91	92	91	91	**91**	**0.4**
3	92	91	91	91	92	**91**	**0.5**
4	92	92	91	90	91	**91**	**0.8**

An IRHD rating of 91 degrees is approximately equivalent to a Shore A hardness of 89A.

Similarly, the hardness of the o-ring insets was measured on the IRHD Micro Compact II hardness tester. The specified hardness of the inset samples was 70A, and the average value from the IRHD measurements was equivalent to 72A.

5.1.6. Long-term Compression Stress Relaxation Test

The tensile tests that were conducted on the molded Flexane samples showed that the compound displayed short-term viscoelastic behavior. To verify that the Flexane material would was also demonstrate long-term viscoelastic behavior, a test stand was fabricated, shown in Figure 15, that imposed a fixed displacement on the o-ring sample and measured the sealing force over time. The o-ring was subjected to a 6% compression, 0.72-mm, for 120-days. Testing was performed at room temperature and pressure.

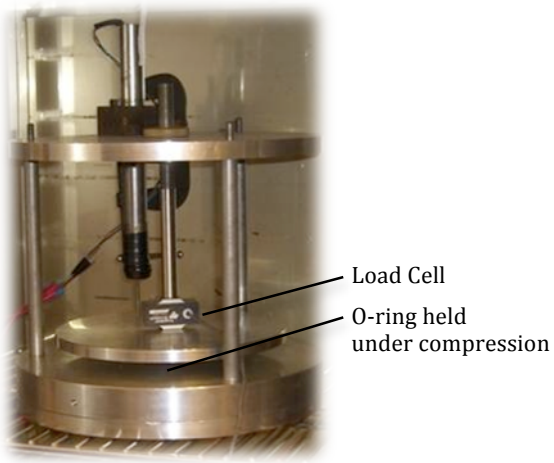

Figure 15: Long-Term CSR Test Stand
The test stand imposed a fixed displacement on o-ring specimens and tracked sealing force over time.

Data points plotted and presented in Figure 16 shows that after 120-days under compression, force decay still occurred, a common property of elastomeric sealing materials [12]. Also noteworthy from the long-term stress-relaxation tests is how well a least-fit logarithmic curve fits the data points. The decay equation was a least-squares logarithmic curve with an R^2 value of 0.963.

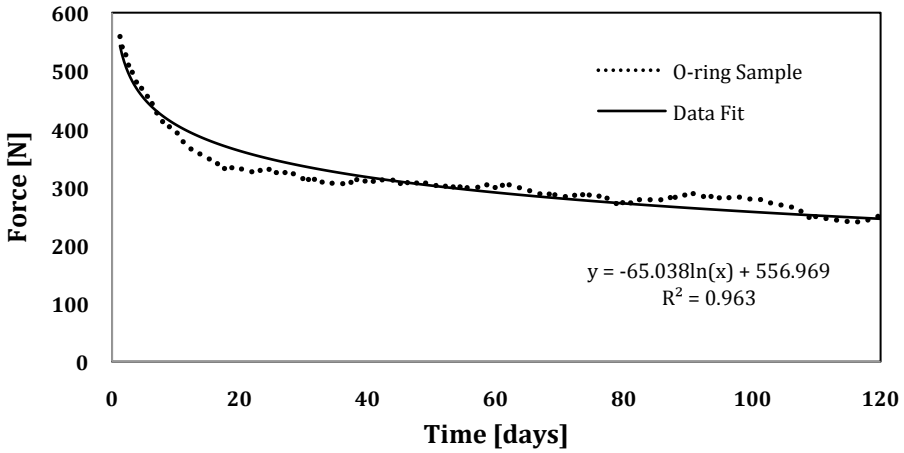

Figure 16: Long-Term O-ring Compression Stress Relaxation

5.2. Compression Set

5.2.1. Test Setup

The compression set test was designed using ASTM D395 guidelines [24] for measuring compression set. These guidelines recommend that samples should be compressed at least 15% of their original thickness, and should be held under compression for 70-hours. Compression set measurements should be taken 30-minutes after the strain is released.

While ASTM guidelines specify measuring compression sets on small disk specimens of the rubber material being used, it was shown by Bigg et al. [14] that the compression set measurements of disks and o-rings of the same material weren't consistently correlated, therefore compression tests were performed and measurements made using the more realistic situation with experimental o-rings.

A compression fixture was designed and fabricated that could hold an entire sample set consisting of four different o-ring designs, and simultaneously impose the same deformation on all samples in the set. The dimensions of each fully cured o-ring sample was recorded before compression, then the specimens were placed in the compression fixture, and the plates were clamped together using fastening bolts. Spacers 2.38-mm in height were used to limit the movement of the clamping plate to the desired 18.75% compression. The compression set test fixture is shown in Figure 17.

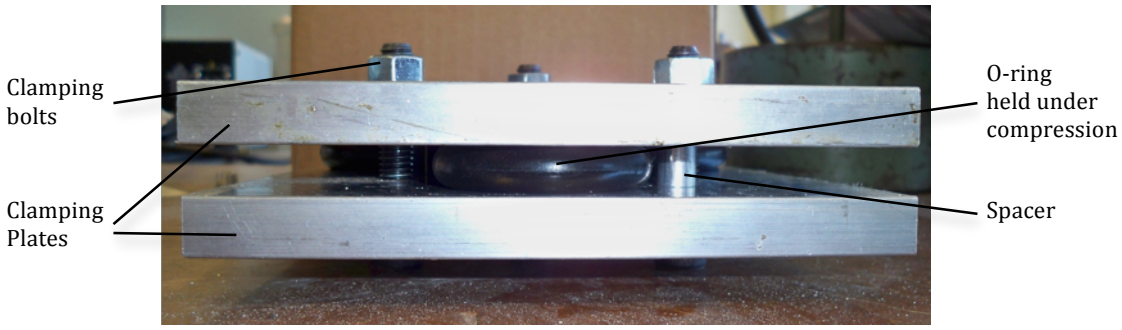

Figure 17: Compression Set Fixture

Accelerated aging is a common practice in stress relaxation and compression testing of elastomers, e.g. as described in the work of Gillen et al. [12]. The same approach was used

in this work. After applying the compression, the o-ring specimens were immediately placed in an oven pre-heated to 45°C, and left for 70-hours.

After removing the fixture from the oven, the o-ring samples were immediately removed from the fixture, and placed on a wooden surface, a poor thermal conductor. The samples were untouched and allowed to relax for 30-minutes, and then final diameter measurements were taken. Results from two sets of compression sets were averaged and are presented in Table 9. The compression set values were plotted and are presented in Figure 18.

5.2.2. Results

The experimental results correspond to the calculated strain energy results described in Section 4, which predicted a decreasing permanent deformation with decreasing strain energy content in the seal. The design with 4-mm insets, the largest insets, exhibited the least compression set. The baseline design o-ring exhibited the largest compression set, 95% compared to the 67% compression set for the 4-mm inset design. The 2-mm and 3-mm inset designs also fall into accordance as expected, demonstrating compression set values of 87% and 78%.

Table 9: Compression Set Results – 18.75% Compression

O-ring Design	*Initial O-ring Diameter [mm]*	*Compressed Diameter [mm]*	*Final Diameter [mm]*	*Compression Set [%]*
Baseline	12.62	10.32	10.52	95%
Modified: 2-mm Insets	12.64	10.32	10.67	87%
Modified: 3-mm Insets	12.62	10.32	10.85	78%
Modified: 4-mm Insets	12.62	10.32	11.05	67%

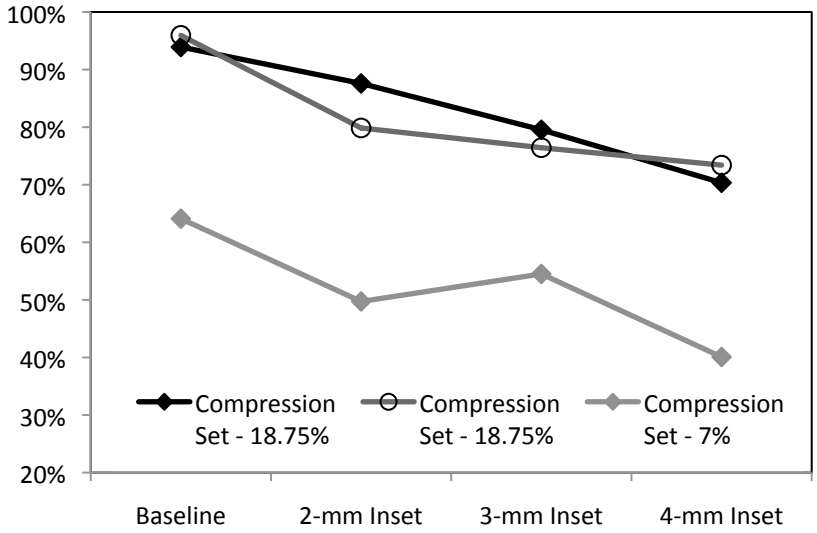

Figure 18: Compression Set Results

A second set of compression set measurements was gathered from o-ring samples that were exposed to long-term stress relaxation tests described in Section 5.3. The data presented in Figure 18 and Table 10 show that the baseline o-ring design made of one homogeneous material exhibits the highest amount of permanent deformation and compression set, 64%, while the 4-mm inset design exhibits the least compression set, at just 40%.

Table 10: Compression Set Results – 7% Compression

O-ring Design	*Initial O-ring Diameter [mm]*	*Compressed Diameter [mm]*	*Final Diameter [mm]*	*Compression Set [%]*
Baseline	12.60	11.72	12.07	64%
Modified: 2-mm Insets	12.65	11.76	12.22	50%
Modified: 3-mm Insets	12.65	11.76	12.17	55%
Modified: 4-mm Insets	12.68	11.72	12.32	40%

5.3. Compression Stress Relaxation

5.3.1. Test Setup

Compression stress relaxation testing of elastomer parts is a very useful tool in order to know exactly how much force the rubber material at a point is exerting at a point in time.

Tracking an o-ring's sealing force over time sheds light on its long-term performance. In this work, the sealing force data collected for different o-ring designs was used to compare the rate of sealing force decay for different seal designs.

Eight o-ring samples were created; two each of four different seal designs. First, a baseline homogeneous design o-ring was created, then the subsequent design o-rings contained two softer insets each, of 2-mm, 3-mm, and 4-mm diameters respectively. An initial sample set of one of each design was created, and several months later, a second sample set was created, again with one o-ring design each.

Stress relaxation tests were performed on a mechanical testing machine at room temperature over a period of 8 to 10 days. The o-rings were held under a fixed 7% displacement, 0.889-mm, and the decay of the seals' reaction force was measured over time.

5.3.2. Results

Sealing force over time for eight o-ring specimens was plotted and the data is shown in Figure 19. An initial group of four o-rings of four different designs, one baseline and three modified designs, was tested, and sealing force plots are shown in black. A second set of o-rings of the same four designs were tests and sealing force plots are shown in blue. The decay of sealing force over time corresponds to expected behavior based on previous work. All samples exhibited very sharp sealing force decay for the first 2-days, and this rate of decay slowed as time moved forward.

It can be seen that both o-ring samples of the baseline design displayed sealing forces over time that were relatively close in value. Similarly, both o-ring samples of the 2-mm inset design showed sealing force values that remain relatively close over time. The samples made of the 3-mm and 4-mm inset o-ring designs showed a larger difference in retained sealing force over time. A method of comparing the performance of each o-ring design is not immediately apparent from studying the force decay plots in Figure 19. To compare o-ring performance, the rate of sealing force decay was investigated from this data.

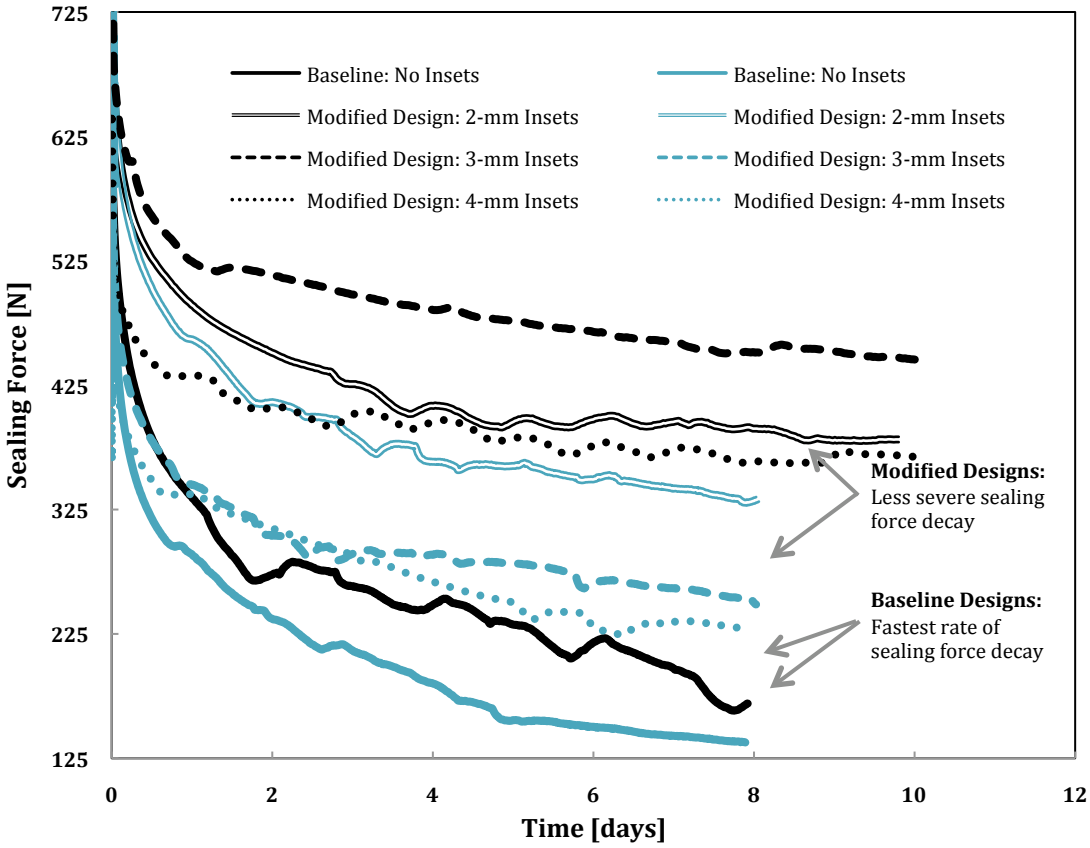

Figure 19: Compression Stress Relaxation Results
An initial set of four different o-ring designs, one baseline, and three modified designs with insets, were conducted and force decay plots are shown in black. A second set of the same four o-ring designs were then observed over time, and the force decay plots shown in blue.

In order to quantitatively compare the different o-ring samples, logarithmic curves were fit to the experimental stress relaxation data. Data points from 1-day to 8-days were isolated for a curve fitting procedure. These curves were used to determine sealing force decay rates for each sample. The logarithmic curves were fit to the data points using a least-squares fit, and each equation was of the form,

$$F(t) = A\ln[t] + B.$$

From this, the rate of change of sealing force over time is,

$$\frac{dF}{dt} = \frac{A}{t}.$$

The rate of decay coefficients, *A*, were used to compare the various samples. In this form, *A* = 0 would describe an ideal o-ring that experiences no sealing force decay over time. All o-ring designs from this experiment were expected to have decay coefficients less than 0. The lowest values of *A* indicated poorly performing seals that exhibited the fastest rates of sealing force decay. The decay coefficients for each pair of o-ring designs were averaged for comparison between the different designs. Even though the sample size consisted of only two specimens of each o-ring design, a standard deviation was calculated for comparison purposes. The decay equations, R^2 values, decay coefficients, average coefficients, and deviations are presented in Table 11. The change from baseline is also calculated for each modified o-ring design.

Table 11: Compression Stress Relaxation Curve Fitting

O-ring Design	*F(t)*	R^2	*Decay Coefficient, A*	*Average Decay Coefficient*	*Standard Deviation*	*Change from Baseline*
Baseline	-66.8 ln[t] + 330	0.900	-66.8	-72.0	7.3	-
Baseline	-77.2 ln[t] + 290	0.989	-77.2			
Modified: 2-mm Insets	-48.5 ln[t] + 481	0.928	-48.5	-53.4	6.9	26%
Modified: 2-mm Insets	-58.3 ln[t] + 452	0.976	-58.3			
Modified: 3-mm Insets	-39.2 ln[t] + 538	0.962	-39.2	-39.0	0.3	46%
Modified: 3-mm Insets	-38.8 ln[t] + 338	0.940	-38.8			
Modified: 4-mm Insets	-30.4 ln[t] + 430	0.922	-30.3	-45.35 †	N/A	37% ††
Modified: 4-mm Insets	-60.4 ln[t] + 340	0.973	-60.4 †			

† The decay coefficient of -60.4 for the 4-mm inset design falls out of line with expected results, causing a lower average decay coefficient than expected for this o-ring design.
†† While 37% for the 4-mm design is an improved sealing force retention rate over the baseline design, a larger difference from the baseline was expected.

The R^2 values from Table 11 show that the logarithmic forms offer acceptable representations of sealing force decay for each sample. When considering the decay coefficient, *A*, to quantify seal performance, the average results fell within expectations for three of the four different o-ring designs. Overall, as the size of the soft inset was increased, the rate of loss of sealing force decreased. This is due to the decreased ESED in the seal that

results from the softer inset. With an average decay coefficient of A = -72, the baseline design exhibited the fastest rate of sealing force decay. With an average decay coefficient of A = -53.4, the 2-mm inset design exhibited a 26% decreased rate of sealing force decay when compared to the baseline. The 3-mm inset design exhibited a force decay rate that was 46% slower than the baseline.

There is a varying degree of deviation in the decay coefficients for the o-ring designs that were tested. For the baseline design, and the 2-mm inset and 3-mm inset modified designs, the standard deviations fell below 7. For the 4-mm inset design, the deviation was 21.3, which does not fall within an acceptable amount of error as exhibited by the other o-ring samples. The decay coefficient of A = -30.3 falls in line with the expected trend, but the decay coefficient of -60.4 does not. By averaging these two values, the 4-mm inset design exhibits a sealing force decay rate that is 37% slower than the baseline, which is a lower than expected.

Three factors are proposed to explain some of the deviation in sealing forces over time, but it is unknown which effect, or combination of effects, is dominant. First, since each o-ring sample was cast from independently mixed batches of the rubber compound, it is possible that there was some unexpected and undocumented variation in the mixing of the casting agent and resin when preparing the compound mixture for the main o-ring. Second, the second set of o-ring samples was created several months after the first, and it is possible that the shelf life of the o-ring insets had some effect on their long-term performance. Further evidence for this possibility can be seen by the fact that all testing conducted on the second set of o-ring samples saw lower initial sealing forces. Third, the testing was conducted at room temperature, and again, it is possible that environmental effects such as room temperature, pressure, and humidity fluctuations could have affected the material responses.

Even with the unexpected deviation in the 4-mm inset design, all six o-rings of modified designs including softer insets exhibited slower rates of sealing force decay over time when compared to the baseline o-ring. These results agree with the proposed theory that correlated the rates of sealing force loss with the strain energy density in the seal.

6. Numerical Simulations – Nonlinear Materials

While the aforementioned results in Sections 4 and 5 show seal-designs including insets with different material behavior that exhibit lower strain energy levels, improved compression set values, and slower rates of stress relaxation compared to baseline designs, it was also seen that the sealing forces and sealing pressures of these designs were decreased. In order to further apply the idea of utilizing material behavior to improve seal design by minimizing strain energy in the seal, further numerical simulations were carried out, and are described in this section, as well as Section 7.

In this section, the effect of using material insets with properties that show nonlinear stress responses to an applied strain is studied. The goals of utilizing these nonlinear material models were to 1) identify the effect that the nonlinearity of different material models had on the amount of strain energy that would occur across the seal cross-section, and how this would affect the generated sealing pressure, 2) use these materials to compensate for a decrease in the maximum potential contact pressure demonstrated in previous o-ring designs, and 3) identify key material behaviors that will continue the pave the way toward utilizing adaptive material behavior to improve seal design.

Two typical nonlinear material responses are strain-stiffening and strain-softening, where a material's stiffness is not represented by a single-valued elastic modulus, E, but changes with the amount of strain that is applied to the material. Many elastomers naturally undergo a moderate to significant stiffening in their stress-strain curves when exposed to strains upwards of 150%. See Figure 20.

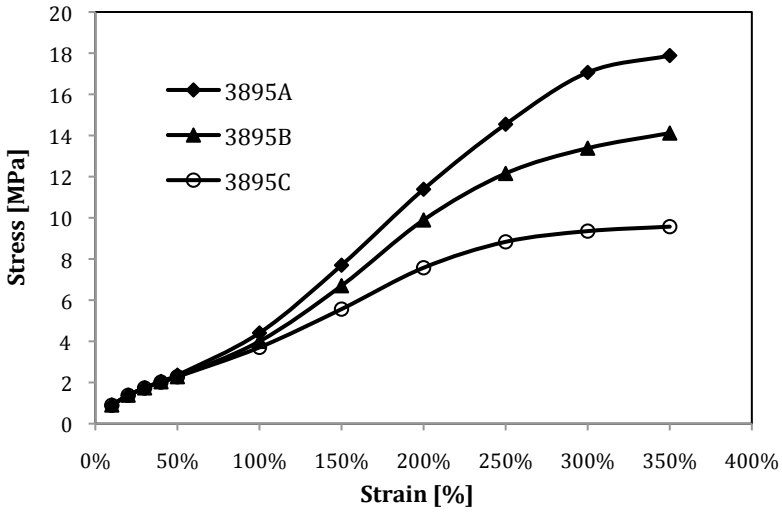

Figure 20: Hyperelastic Stress-Strain Response of Various Rubbers
Tensile stress response of various rubber compounds received from Precision Associates Inc. of Minneapolis, Minnesota. The three different elastomer materials contained varying amounts of carbon black, which affected the rubber's stress response above 100% strain. The 3895A compound experienced a sharp strain-stiffening between 100 and 250% strain, while the 3895C compound exhibited moderate strain-stiffening above 100% strain, and severe strain softening between 200 and 350% strain. See Appendix C for test data.

6.1. Hyperelastic Material Modeling

As shown in Figure 20, the strain-stiffening that is observed in many elastomeric materials occurs at very large strains. Material models were investigated where this strain-stiffening behavior would occur at much lower strains, and thus have an effect in o-ring loading cases on the order of an approximate 15% compression seen in real sealing applications. These material models were confined to the inset materials.

Hyperelasticity provides a means of modeling the stress-strain behavior of elastomer materials whose stress-strain relationship is non-linearly elastic. The assumption is that the stress state of a material can be defined at any point in the body if the state of deformation, or strain, is known. The behavior of these materials is derived from the strain energy potential function, *W*, [25] which is a scalar function of the strain tensor,

$$S_{ij} = \frac{\partial W}{\partial E_{ij}} = 2\frac{\partial W}{\partial C_{ij}},$$

where,

S_{ij} represents the components of the 2nd Piola-Kirchoff stress tensor,
W is the strain energy per undeformed volume,
E_{ij} represents the components of the Lagrangian strain tensor,
C_{ij} represents the components of the right Cauchy-Green deformation tensor.

The Lagrangian strain tensor is expressed as,

$$E_{ij} = \frac{1}{2}(C_{ij} - \delta_{ij}),$$

where δ_{ij} is the Kronecker delta, and represents the identity matrix. The Cauchy-Green deformation tensor is expressed as,

$$C_{ij} = F_{ij}F_{kj},$$

where F_{ij} represents the components of the deformation gradient tensor. It follows that,

$$J = \det\left|F_{ij}\right| = \frac{dV}{dV_o},$$

where J, the Jacobian, is the ratio of the deformed volume to the original undeformed volume.

The squared principal stretch ratios [Figure 21] are the eigenvalues of the Cauchy-Green deformation tensor. The eigenvalues exist only if,

$$\det\left|Cij - \lambda_p^2 \delta ij\right| = 0,$$

where,

$$\lambda i = \frac{l_i + dl_i}{l_i} = 1 + \varepsilon_i.$$

This can be expressed as,

$$\lambda_p^6 - I_1\lambda_p^4 + I_2\lambda_p^2 - I_3 = 0,$$

where I_1, I_2, and I_3 are referred to as the principal invariants of C_{ij}.

$$I_1 = \lambda_1^2 + \lambda_2^2 + \lambda_3^2,$$
$$I_2 = \lambda_1^2\lambda_2^2 + \lambda_2^2\lambda_3^2 + \lambda_3^2\lambda_1^2,$$
$$I_3 = \lambda_1^2\lambda_2^2\lambda_3^2.$$

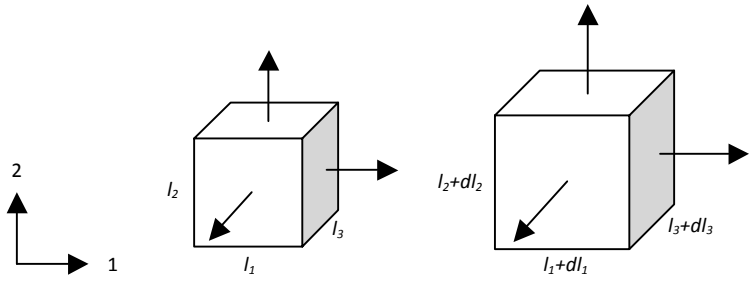

Figure 21: Principal Stretch Ratios

The principal stretch ratios, λ_i, are defined as the ratio of stretched length to unstretched length of the edges of an infinitesimal undeformed volume element.

For purely incompressible materials, $I_3 = 1$. If an isotropic material response is acceptable for the material model, the strain energy potential function can be expressed in terms of the strain invariants and the Jacobian as follows,

$$W = W(I_1, I_2, J).$$

Several hyperelastic material models have been developed, including the Arruda-Boyce, Neo-Hookean, Mooney-Rivlin, Ogden, Polynomial, and Yeoh models. The first two are models derived from arguments underlying the structure of the material. The other models

are empirical material descriptions. Many finite element packages now offer the capability of importing material testing data from various types of stress-strain mechanical tests and offer curve-fitting procedures to characterize material response in relation to one of the aforementioned models. Typical testing modes utilized to generate data for creating hyperelastic material models are shown in Figure 22. The curve fitting procedures are sensitive to data input, and if the material model and geometry and/or application are incompatible, instabilities can result in program locking, or erroneous results can be generated [26]. The accuracy of the material response is also compromised if insufficient material testing data is input.

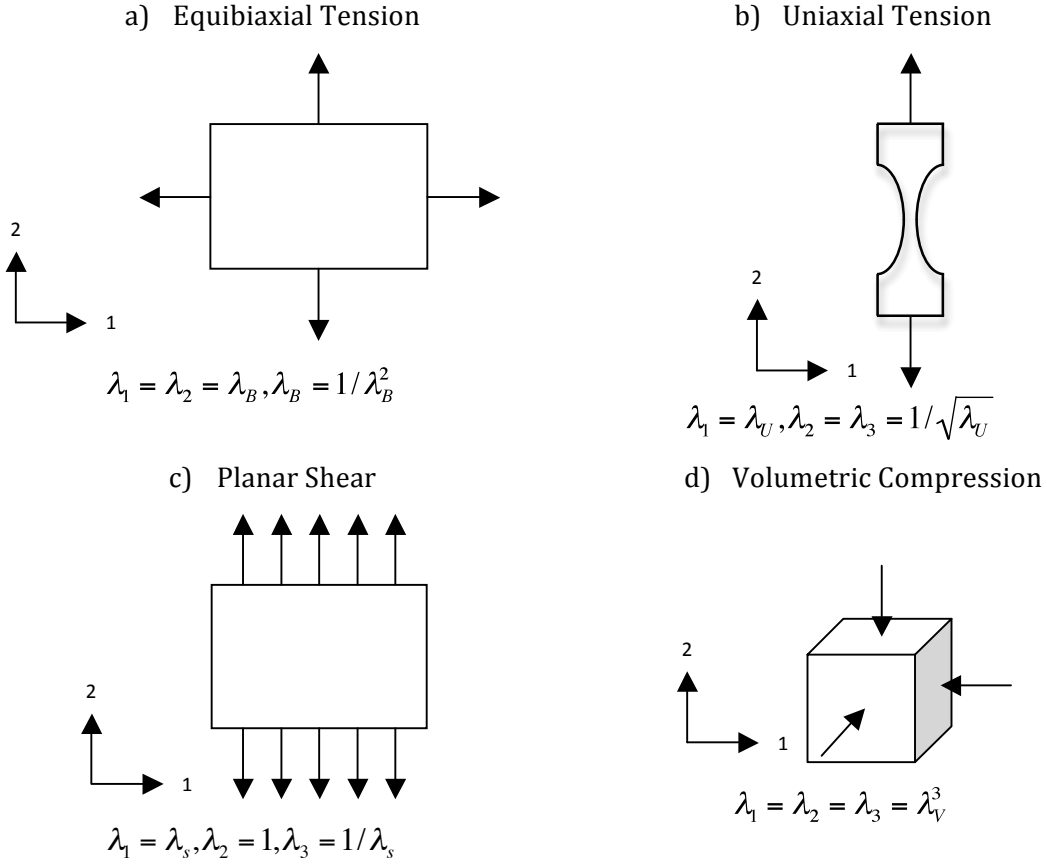

Figure 22: Types of Material Testing

The Mooney-Rivlin model was chosen for this work. The FEA package used offers the option of a 2, 3, 5, or 9-term Mooney-Rivlin model. The 9-term model was used because of

the inflection points in the stress-strain data, and it was seen that the generated material coefficients had low residual values. The 9-term model is,

$$W = c_{10}(\overline{I}_1 - 3) + c_{01}(\overline{I}_2 - 3) + c_{20}(\overline{I}_1 - 3)^2 + c_{11}(\overline{I}_1 - 3)(\overline{I}_2 - 3) + c_{02}(\overline{I}_2 - 3)^2 + c_{30}(\overline{I}_1 - 3)^3$$
$$+c_{21}(\overline{I}_1 - 3)^2(\overline{I}_2 - 3) + c_{12}(\overline{I}_1 - 3)(\overline{I}_2 - 3)^2 + c_{03}(\overline{I}_2 - 3)^3 + \frac{1}{d}(J-1)^2,$$

where c_{10}, c_{01}, c_{20}, c_{11}, c_{02}, c_{30}, c_{21}, c_{12}, c_{03}, and d, are material constants. These constants are regression coefficients determined by the input material data.

6.2. Numerical Simulations

The models for FEA analysis were similar to those used in other studies described in Section 4. An axisymmetric model was setup in the software package. The dimensions of the o-ring model for these new simulations matched those of the experimental o-rings that were created and described in Section 5. The o-ring cross-section was 12.7-mm in diameter, and the o-ring had an inner diameter of 25.4-mm. The o-ring model contained two 3-mm insets that were placed in the region of predicted highest ESED determined from previous numerical simulations. In the model, the center of the inset was offset 3.49-mm from the center of the o-ring cross-section. The entire seal cross-section was meshed with 29525 Plane 182 quad node elements. A Poisson's ratio of 0.495 was used for both the main o-ring material and inset material model. The glands were given an elastic modulus of 210-GPa and a Poisson's ratio of 0.3. Contact pairs were created at both the upper and lower seal-gland interfaces, with the o-ring being assigned 372 contact elements and the gland being assigned rigid target elements. As in the previous numerical simulations, a friction coefficient of 0.24 was defined between the contacting surfaces of the o-ring and gland.

A displacement of 1.905-mm was applied to the upper gland, which compressed the o-ring by 15% of its diameter. The simulation was setup with a single time-independent load step that was divided into 300 substeps.

Two materials with linear material behavior were created as baseline materials. Material 6, with an elastic modulus of 4-MPa and a Poisson's ratio of 0.495, was used as the main o-ring material in all simulations. The other baseline material, Material 1, had an elastic modulus of 3-MPa, and a Poisson's ratio of 0.495. A range of material test data for natural rubber was reviewed in the literature (such as Drozdov and deClaville Christiansex [27]) in order to observe the strain-stiffening responses to the different types of strain loadings described above. Material models based on Material 1 were created that exhibited strain-stiffening in the different test modes shown in Figure 22. The shape of the various stress-strain curves, i.e. the amount of strain-stiffening that was experienced in the material behavior, was subsequently modified in different material models. An example of material test data created to develop material models for the simulations is shown in Figure 23. This material was labeled Material 12.

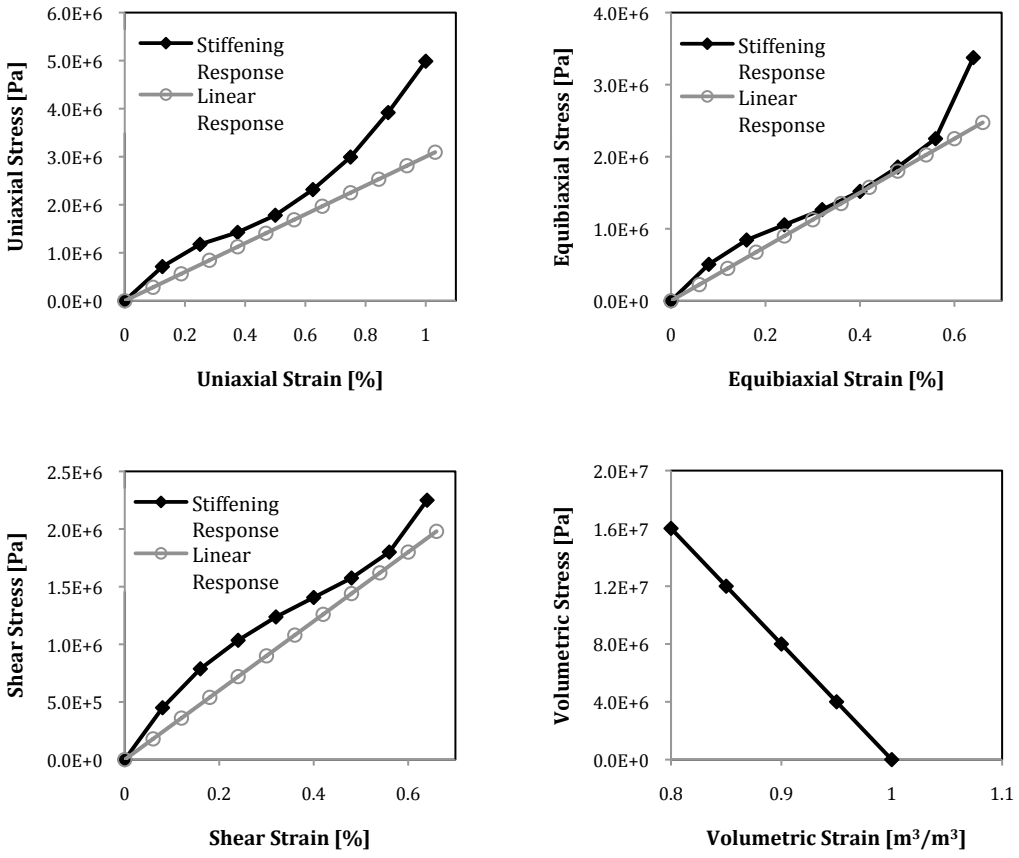

Figure 23: Sample Material Model – Material 12
Testing data used to create one of the material models to be used in o-ring designs.

For all material models, the created material test data were imported into the commercial FEA package, and 9-parameter Mooney-Rivlin material models were developed. The material constants for a sample material model, Material 12, are shown in Table 12.

Table 12: Mooney-Rivlin Model Constants – Material 12

Material Constant	*Value*
c_{10}	1429675.25
c_{01}	-614131.23
c_{20}	224676.34
c_{11}	-1219576.60
c_{02}	782420.74
c_{30}	-487774.66
c_{21}	1748675.31
c_{12}	-1462421.99
c_{03}	320236.96
d	2.506 E-8
Residual	0.0796

Table 13 and Table 14 present descriptions of all the material models that were utilized in the numerical simulations. The material numbers are simply a labeling convention developed for differentiating the materials, and do not represent any physical properties of the material.

Table 13: Hyperelastic Material Models

Material No.	*Description*
Material 6	Linear Material Model – E = 4.0-MPa -Used as main o-ring material in all designs -Used for homogeneous single material baseline
Material 1	Linear Material Model – E = 3.0-MPa -Used as base for strain-stiffening material models
Material 12	Based on Material 1 -All strain-stiffening reduced by 28.75%
Material 11	Based on Material 12 -All strain-stiffening reduced by 10%
Material 1061	Based on Material 12 -All maximum stress values decreased by 35%
Material 1062	Based on Material 12 -All maximum stress values decreased by 40%
Material 10608	Based on Material 1061 -Biaxial & shear strain-stiffening decreased by 10%
Material 10609	Based on Material 1061 -Biaxial & shear strain-stiffening decreased by 5%
Material 106101	Based on Material 1061 -Volumetric strain-stiffening increased by 25%
Material 10611	Based on Material 1061 -Biaxial max stress increased by 15% -Shear max stress increased by 30%
Material 10612	Based on Material 10611 -Biaxial max stress increased by 15% -Shear max stress increased by 30%
Material 10619	Based on Material 10612 -Volumetric strain-stiffening increased 10%
Material 10617	Based on Material 10612 -Volumetric strain-stiffening increased 15%
Material 10618	Based on Material 10612 -Volumetric strain-stiffening increased 20%
Material 10613	Based on Material 10612 -Volumetric strain-stiffening increased 25%
Material 10615	Based on Material 10612 -Volumetric strain-stiffening increased 30%
Material 10616	Based on Material 10612 -Volumetric strain-stiffening increased 35%
Material 10614	Based on Material 10612 -Volumetric strain-stiffening decreased by 25%
Material 107	Based on Material 12 -All strain-stiffening reduced by 30%
Material 108	Based on Material 12 -All strain-stiffening reduced by 20%

Table 14: Hyperelastic Material Models

Material No.	*Description*
Material 115	Based on Material 12 -All strain-stiffening reduced by 5%
Material 11505	Based on Material 115 -Volumetric strain-stiffening decreased by 30%
Material 11506	Based on Material 115 -Volumetric strain-stiffening decreased by 25%
Material 11507	Based on Material 115 -Volumetric strain-stiffening decreased by 20%
Material 11508	Based on Material 115 -Volumetric strain-stiffening decreased by 15%
Material 11509	Based on Material 115 -Volumetric strain-stiffening decreased by 10%
Material 11510	Based on Material 115 -Volumetric strain-stiffening decreased by 5%
Material 11511	Based on Material 115 -Volumetric strain-stiffening increased by 10%
Material 11512	Based on Material 115 -Volumetric strain-stiffening increased by 15%
Material 11513	Based on Material 115 -Volumetric strain-stiffening increased by 20%
Material 11514	Based on Material 115 -Volumetric strain-stiffening increased by 25%
Material 11515	Based on Material 115 -Volumetric strain-stiffening increased by 30%
Material 11516	Based on Material 115 -Volumetric strain-stiffening increased by 35%
Material 11524	Based on Material 115 -Biaxial strain-stiffening decreased by 10%
Material 11526	Based on Material 115 -Biaxial strain-stiffening increased by 10%
Material 11527	Based on Material 115 -Biaxial strain-stiffening increased by 15%
Material 11528	Based on Material 115 -Biaxial strain-stiffening increased by 25%
Material 11534	Based on Material 115 -Shear strain-stiffening decreased by 10%
Material 11536	Based on Material 115 -Shear strain-stiffening increased by 10%
Material 11537	Based on Material 115 -Shear strain-stiffening increased by 15%
Material 11538	Based on Material 115 -Shear strain-stiffening increased by 20%
Material 11544	Based on Material 115 -Uniaxial strain-stiffening decreased by 5%
Material 11546	Based on Material 115 -Uniaxial strain-stiffening increased by 5%
Material 11547	Based on Material 115 -Uniaxial strain-stiffening increased by 10%
Material 11549	Based on Material 115 -Uniaxial strain-stiffening increased by 20%

Similar to the investigations described in Section 4, the two main mechanical quantities chosen for analysis were ESED contour plots and maximum contact pressure. The FEA

package used could not generate contour plots for elements with hyperelastic material properties. As ESED contour plots were important in quantifying the strain energy content of the o-ring designs for comparison between different designs, various manual computational methods were attempted to determine an approximate ESED value that could be used to generate contour plots. Using the results from a baseline o-ring design with linear material properties, various ESED computations were compared to software calculated results for the simulations in Section 4. The approach that gave the most precise approximation for different o-ring designs, and was also closest to the software calculated ESED, was as follows:

$$ESED = u = \frac{1}{2}\sigma_{VM}\varepsilon_{VM},$$

using software calculated values of Von Mises stress and Von Mises strain, σ_{VM} and ε_{VM}.

This value is the approximate elastic strain energy density per element, and these values computed for each element were used to generate contour plots similar to those utilized in Section 4. The contour plots were used to compute the ESED intensity, the dimensionless value created to numerically quantify the amount of energy stored in the seal. The technique to compute the ESED intensity with the aid of imaging software was previously detailed in Section 4.2.2. In summary, ESED intensity was calculated by multiplying the average strain energy density in each contour color in the FEA generated plots by the area of the contour then summing the results for all contours. The contour area was defined as the number of pixels in each contour and was determined with the use of imaging software.

6.2.1. Results

After the numerical simulations were completed, the maximum contact pressures, and ESED intensities were tabulated and analyzed. The baseline design for these simulations was an o-ring made of Material 6, a linear material model with an elastic modulus of 4.0-MPa. To more conveniently analyze the balance between ESED intensity values and maximum contact pressure for each o-ring design, all quantities for all designs were normalized by the ESED intensity and maximum contact pressure of the baseline design. For the baseline

design o-ring made from Material 6, the ESED intensity was 2.79, and the maximum contact pressure was 1.145-MPa.

The amount by which contact pressure changed was compared to the amount by which ESED intensity changed for each design. A performance metric, M_p, was defined as

$$M_P = \frac{ESEDI_{VM\_baseline} - ESEDI_{VM\_new\_design}}{ESED_{VM\_baseline}} - \frac{CP_{baseline} - CP_{new\_design}}{CP_{baseline}}.$$

The performance metric M_p includes values of both ESED intensity and maximum contact pressure, and was defined so that a value of 0% would indicate an o-ring design that performs exactly as the baseline, values greater than 0% are improved o-ring designs, and values less than 0% are o-ring designs that exhibit a decrease in performance.

A sampling of the data from the numerical studies is presented in Table 15 to demonstrate the method. Many of the initial material models incorporated into the o-ring design were unsuccessful in increasing the maximum potential sealing pressure to a value near that of the baseline design. In addition to this, in all cases, the material behavior modifications led to even greater increases in the ESED intensity across the seal cross-section. However, the o-ring design utilizing Material 115 for the insets resulted in a performance metric, M_p, of -0.485%, very close to the baseline performance metric. It was determined that this material model was worth investigating further. Modifications were made to the material model so that its incorporation into o-ring designs would yield an increased performance metric.

Table 15: Results: Hyperelastic Material Models

Simulation No.	*1*	*2*	*3*	*4*	*5*	*41*
O-ring Design Main - Inset	6*	6 - 1	6 - 1062	6 - 10608	6 - 10609	6 – 115
$Stress_{VM\text{-}Max}$ [MPa]	0.872405	0.877489	0.877297	0.865377	0.864757	0.948169
CP_{Max} [MPa]	1.144744	0.978171	0.943486	0.975782	0.977227	1.209546
ESED Intensity	2.790	2.613	2.670	2.712	2.707	2.961
$ESEDI_N$	1.0	0.937	0.957	0.972	0.970	1.062
CP_N	1.0	0.854	0.824	0.852	0.854	1.057
CP_N / $ESEDI_N$	1.0	0.912	0.861	0.877	0.880	0.996
M_p	0%	-8.21%	-13.30%	-11.97%	-11.66%	-0.485%

The 6* notation indicates the baseline design made of a single homogeneous linear material. CP_N is the normalized maximum contact pressure. $ESEDI_N$ is the normalized ESED intensity.

New material models were made and additional analysis was conducted. Given the complex state of stress that develops in an o-ring under compression between two parallel glands, i.e. vertical, horizontal, and shear stresses, material behavior was modified so that stiffness would vary depending on the type of loading being applied. For example, two material models, A and B, could behave similarly in a uniaxial loading, but respond differently in an equibiaxial or shear loading. With the development of new material models with behavioral modifications, a very interesting trend was observed. The behavior of the material could serve as a mode of increasing maximum potential sealing pressure. Additional material models were created based on Material 115. In each new material model, the material's biaxial strain-stiffening response and shear strain-stiffening response were isolated and individually modified. The data points of the material models were increased or decreased slightly more than Material 115. As an example, the stress-strain response for an equibiaxial loading on Material 115, 11524, and 11528 are shown in Table 16. The data from Table 16 as well as equibiaxial and shear stress-strain data for other material models based on Material 115 are shown in Figure 24.

Table 16: Sample Equibiaxial Stress-Strain Data

Equibiaxial Strain *[%]*	*Equibiaxial Stress Material 115* *[Pa]*	*Equibiaxial Stress Material 11524* *[Pa]*	*Equibiaxial Stress Material 11528* *[Pa]*
0	0	0	0
0.08	480938	432844	601172
0.16	801563	721406	1001953
0.24	1001953	901758	1252441
0.32	1202344	1082109	1502930
0.40	1442813	1298531	1803516
0.48	1763438	1587094	2204297
0.56	2137499	1923750	2671874
0.64	3206250	2885625	4007813

Sample equibiaxial stress-strain data used to create material models based on Material 115. Material 11524 stress values are 10% less than those of Material 115. Material 11528 stress values are 25% more than those of Material 115.

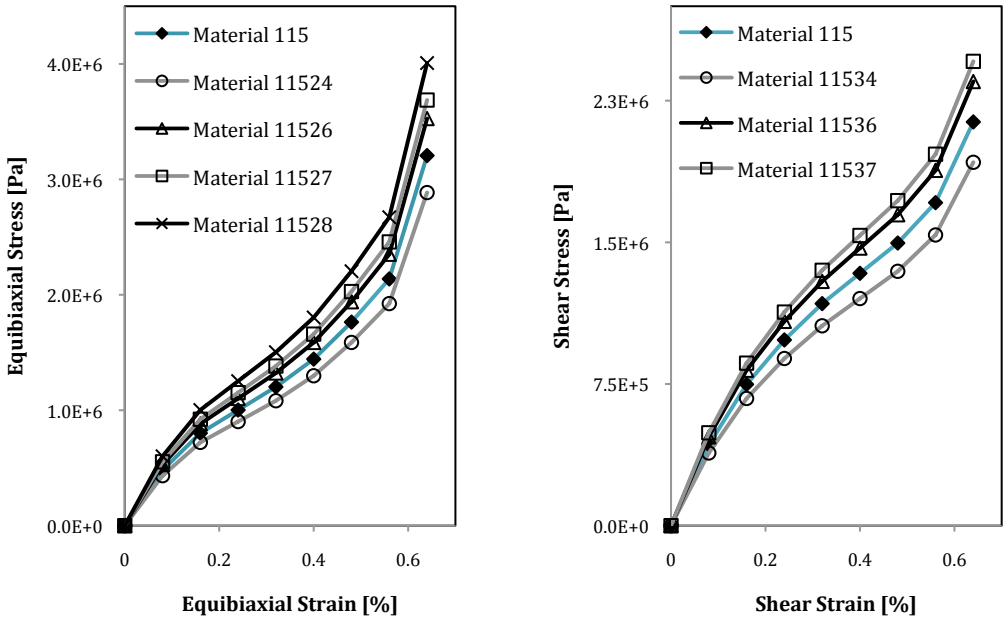

Figure 24: Equibiaxial and Shear Strain-Stiffening Material Data
Material 115, shown in blue, was used as a baseline model to create new material models, where the equibiaxial and shear strain-stiffening behavior was modified.

Simulation results showed that some o-ring designs that have insets with material properties of the material models created from data in Figure 24 exhibit maximum contact

pressures that increase at a larger rate than the amount of strain energy content in the seal, as quantified by the ESED intensity. Results for designs incorporating modified biaxial strain-stiffening and shear strain-stiffening are presented in Table 17 and Table 18 respectively.

For the simulations where the material biaxial strain-stiffening response was modified [Table 17], it was observed that the maximum contact pressure increased in each case, and was greater than the baseline design made of Material 6. The design utilizing decreased equibiaxial strain-stiffening (Material 11524) in the inset region exhibited an increased maximum contact pressure, but exhibited an even greater increase in the strain energy intensity, resulting in a low performance metric, M_p = -1.6%. When materials with increased equibiaxial strain-stiffening (Materials 11526, 11527, and 11528) were used as insets, the maximum contact pressure increased, and for these o-ring designs, the contact pressure increased a larger amount than that of the ESED intensity, resulting in positive performance metrics of 0.2%, 0.5%, and 1.2%.

Table 17: Results – Modified Equibiaxial Strain-Stiffening

Simulation No.	*1*	*41*	*42*	*43*	*44*	*45*
O-ring Design Main - Inset	6*	6 - 115	6 - 11524	6 - 11526	6 - 11527	6 - 11528
$Stress_{VM\text{-}Max}$ [MPa]	0.872405	0.948169	0.943277	0.953881	0.956999	0.963594
CP_{Max} [MPa]	1.144744	1.209546	1.191321	1.225782	1.232919	1.246545
ESED Intensity	2.790	2.961	2.948	2.982	2.992	3.004
$ESEDI_N$	1.0	1.0615	1.0565	1.0687	1.0724	1.0766
CP_N	1.0	1.0566	1.0407	1.0708	1.0770	1.0889
CP_N / $ESEDI_N$	1.0	0.9954	0.9850	1.0020	1.0043	1.0114
M_p	0%	-0.485%	-1.583%	0.213%	0.461%	1.229%

The 6* notation indicates the baseline design made of a single homogeneous linear material. CP_N is the normalized maximum contact pressure. $ESEDI_N$ is the normalized ESED intensity.

For the simulations where the material shear strain-stiffening response was modified [Table 18], the design utilizing decreased shear strain-stiffening (Material 11534) in the inset region exhibited a low performance metric, M_p = -2.1%. When materials with

increased shear strain-stiffening behavior (Materials 11536, 11537, and 11538) were used as insets, the maximum contact pressure increased, and for these o-ring designs, the contact pressure increased a larger amount than that of the ESED intensity when compared to the baseline o-ring design made from Material 6, resulting in positive performance metrics of 0.5%, 1.1%, and 1.7%.

Table 18: Results – Modified Shear Strain-Stiffening

Simulation No.	*1*	*46*	*47*	*48*	*49*
O-ring Design Main - Inset	6*	6 - 11534	6 - 11536	6 - 11537	6 - 11538
$Stress_{VM\text{-}Max}$ [MPa]	0.872405	0.907562	0.980575	0.994228	1.006607
CP_{Max} [MPa]	1.144744	1.170162	1.241055	1.254357	1.266453
ESED Intensity	2.790	2.911	3.012	3.027	3.040
$ESEDI_N$	1.000	1.0434	1.0795	1.0850	1.0895
CP_N	1.000	1.0222	1.0841	1.0958	1.1063
CP_N / $ESEDI_N$	1.000	0.9797	1.0043	1.0099	1.0154
M_p	0%	-2.117%	0.462%	1.077%	1.679%

The 6* notation indicates the baseline design made of a single homogeneous linear material. CP_N is the normalized maximum contact pressure. $ESEDI_N$ is the normalized ESED intensity.

In summary, utilizing material models that exhibit strain-stiffening at relatively low strain values was proposed as a method of balancing the amount of strain energy content and sealing pressure of an o-ring design. Hyperelastic material models were created and utilized as insets in o-ring designs. The developed performance metric, M_p, indicated which o-ring designs produced a greater increase in seal contact pressure than the increase in strain energy content of the seal. Material models were created where equibiaxial and shear strain-stiffening were isolated and modified. As presented in Table 17 and Table 18, o-ring designs utilizing these materials as inset materials demonstrated greater performance metrics, 1.3% and 1.7%, when compared to the established baseline design with a performance metric of 0%.

7. Numerical Simulations – Time-Dependent Material Behavior

An important consideration in the numerical modeling of elastomer and polymer materials is their viscoelastic properties. Even though steady state numerical simulations provide a useful representation of the sealing stress and strain states, and resulting strain energy for the intent of o-ring designs being analyzed in this work, they do not take into consideration the viscoelastic behavior, i.e. the time-dependent material response, of the material under strain.

To apply the concepts of improved seal design based on material property modification through the seal cross-section, it is worthwhile to perform numerical simulations that can be used to compare the performance of different seal designs over a period of time. In Sections 4, 5, and 6, o-ring design was approached with the intent to minimize the strain energy content in the seal cross-section. However, the stored energy in the seal is the driving contributor to the elastomer's ability to perform its sealing function. The work in Section 6 addressed the issue of creating seal designs that minimize strain energy content compared to baseline designs, while maintaining an acceptable amount of contact pressure compared to the baseline. The work described in this section addresses the seal's ability to maintain this level of stored energy over time.

To accomplish this, the goals of this part of the research were to 1) track the stored strain energy in a seal over time in use, 2) track the maximum contact pressure of the seal over time, and 3) demonstrate the usefulness of adaptive material behavior in a portion of the seal cross-section to compensate for contact pressure decay as the seal experiences compression stress relaxation due to its viscoelastic properties.

7.1. Viscoelastic Materials

There are two time-dependent effects exhibited by viscoelastic materials. The first is a time dependent shear modulus, *G(t)*, which describes the material's shear stress vs. shear strain

response, and the second is a time-dependent bulk modulus, *K(t)*, which describes the material's volumetric stress vs. volumetric strain response. As previously stated, elastomers are effectively incompressible, therefore the time-dependent *K(t)* is taken to be a constant in this analysis.

A material's shear modulus and elastic modulus are related by the following [5],

$$G(t) = \frac{E(t)}{2(1+\nu)}.$$

Three viscoelastic material models, Material V6, V5, and V4, were created based on measured long-term compression stress-relaxation data collected and presented in Figure 16 in Section 5.1.6. The data points from Figure 16 were multiplied by constants so that Material V6, V5, and V4, had initial elastic moduli of 4-MPa, 3.8-MPa, and 3.6-MPa, respectively. The elastic moduli of these three material models after 100-days were 3.2-MPa, 3.1-MPa, and 3.0-MPa, respectively. A Poisson's ratio of 0.495 was used and shear modulus values were calculated from the time-dependent elastic modulus. Shear modulus over time, *G(t)*, for the three material models, V6, V5, and V4, is shown in Figure 25.

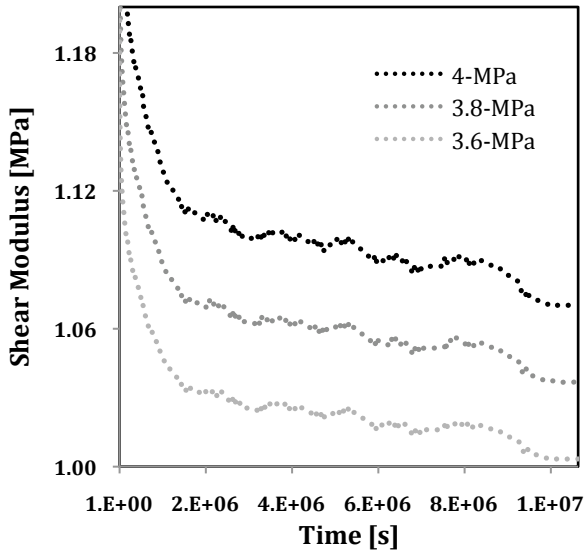

Figure 25: Material Shear Modulus Data for Viscoelastic Material Models
Long-term behavior of three materials models V6, V5, and V4, with starting elastic moduli of 4-MPa, 3.8-MPa, and 3.6-MPa. Plot describes behavior for a period of 100-days.

In order to simulate the effect of the viscoelastic material behavior described in Figure 25 in o-ring designs, a material model was needed to use in the FEA package. A well-established form of the constitutive equations that represent viscoelastic behavior for material analysis is the Prony series [28]. The material model is represented by,

$$G(t) = G_o \cdot (1 - \sum_{i=1}^{N} \alpha_i (1 - e^{\frac{-t}{\tau_i}})),$$

where,

$G(t)$ is the time dependent shear modulus,

G_o is the initial shear modulus,

N is the number of terms in the series,

i is the counting index,

t is the time variable,

α_i are material constants describing the nature of shear modulus decay,

and τ_i are time constants describing the time scale of modulus decay, where α_i and τ_i are determined from experimental data.

The FEA package used contained curve fitting capabilities that determined the constants α_i and τ_i through a nonlinear regression method based on shear modulus over time, $G(t)$. The shear modulus data points use in Figure 25 were imported into the FEA package, and an 8-term Prony series material model was used. With approximate initial coefficient values chosen from the scale of the material shear modulus and time scale data points, the material models were generated for a reference temperature of 25°C. The material constants for the imported data are presented in Table 19.

Table 19: Prony Constants for Viscoelastic Material Models

Material Label	*V6*	*V5*	*V4*
Prony Constants	E_o = 4-MPa	E_o = 3.8-MPa	E_o = 3.6-MPa
α_1	6.777 E-11	5.857 E-11	5.878 E-11
τ_1	1	10	1
α_2	6.777 E-11	2.540 E-14	5.878 E-11
τ_2	10	100	10
α_3	1.416 E-17	0.0363	2.396 E-14
τ_3	100	1000.1	100
α_4	0.0394	0.0303	0.0326
τ_4	1000.1	10000	1000.1
α_5	0.0324	0.0383	0.0277
τ_5	10000	1.0 E5	10000
α_6	0.0418	0.0627	0.0345
τ_6	1.0 E5	1.0 E6	1.0 E 5
α_7	0.0677	0.0259	0.0568
τ_7	1.0 E6	1.0 E7	1.0 E6
α_8	6.777 E-11	5.857 E-11	0.0235
τ_8	1.0 E7	1	1.0 E7

7.1.1. Numerical Model Development

Similar to the work described in previous sections, an axisymmetric o-ring model was setup in the FEA package. The o-ring dimensions were based on the experimental o-ring samples described in Section 5. The cross-section diameter was 12.7-mm and the inner diameter

was 25.4-mm. The o-ring model contained two 3-mm insets placed in the region of highest ESED determined from previous numerical simulations, and the center of the inset was offset 3.49-mm from the center of the o-ring cross-section. The model was meshed with 29525 Plane 182 quad node elements. The glands were given an elastic modulus of 210-GPa and a Poisson's ratio of 0.3. Contact pairs were created at the upper and lower seal-gland interfaces, with the o-ring surface being assigned 372 contact elements and the gland being assigned rigid target elements. As in previous simulations, a friction coefficient of 0.24 was defined between the contacting surfaces.

For the loading, the bottom gland was fixed to have no vertical or horizontal movement, and the top gland was by 1.26-mm to simulate the movement of the o-ring gland compressing the o-ring 15% of its original diameter.

7.1.2. Numerical Simulations

It was determined in previous work described in Section 4 that in an o-ring with insets of a less stiff material, the highest areas of ESED occur right at the o-ring and inset boundary. To compare the different o-ring designs, four specific elements were monitored; three elements tracked ESED over time, and the fourth tracked maximum contact pressure over time. The locations chosen to track ESED were 1) an element of the main o-ring just outside the o-ring/inset boundary, 2) an element in the middle of the o-ring where ESED is relatively high, and 3) an element in the middle of the inset. Contact pressure was tracked by an element at the center of the contact area between the o-ring and the gland. The locations of the elements tracked are presented in Figure 26.

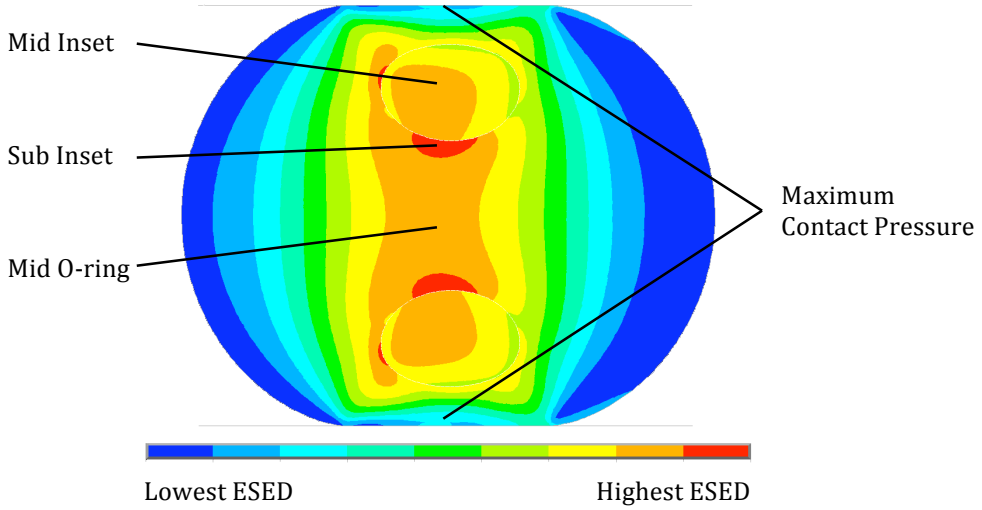

Figure 26: Locations for Tracking ESED and CP Over Time
ESED plot for an o-ring design including insets that are less-stiff than main o-ring materials. ESED was tracked in the three regions: 1) the middle of the o-ring, 2) the region just outside the main o-ring and inset boundary, and 3) in the middle of the inset. Maximum contact pressure was tracked at the center of the contact area between the o-ring and gland interface.

The simulated o-ring application consisted of two load steps. The first load step consisted of a ramped loading, where the 15% compression was applied gradually over 1-second. The second load step held the constant 15% compression on the o-ring for 100-days. Two groups of simulations were conducted. Group 1 simulations investigated o-ring designs whose primary material was viscoelastic, and included an inset that no time-dependent behavior. Group 2 simulations investigated o-ring designs that had viscoelastic behavior, but contained an inset that exhibited adaptive-stiffening behavior, as will be described in Section 7.2. Material distribution for the two groups of simulations is shown in Figure 27.

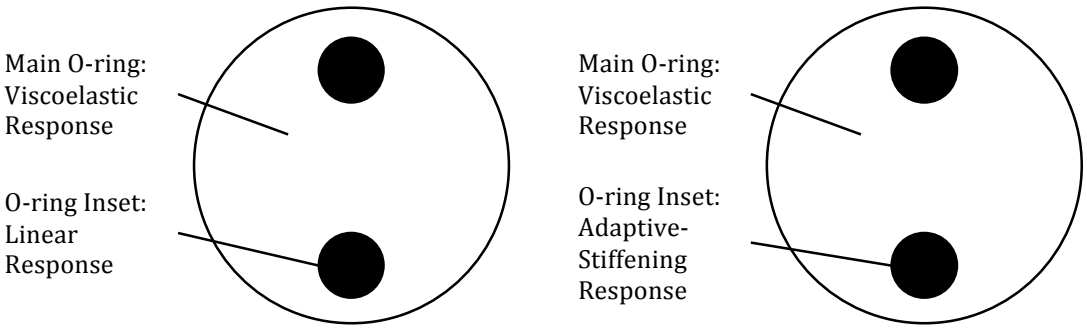

Figure 27: Viscoelastic Numerical Simulation Models
Left: O-ring designs of Group 1 simulations; Right: O-ring designs of Group 2 simulations.

7.2. Adaptive-Stiffening Materials

Figure 28 shows contour plots of the Von Mises stress over time for an o-ring design made from viscoelastic material V5, with a linear elastic modulus of 3.0-MPa. As the state of stress becomes less severe over time, so does ESED. This continuous decrease in stored energy in the seal causes sealing force and sealing pressure losses, as seen in the experimental results in Section 5.

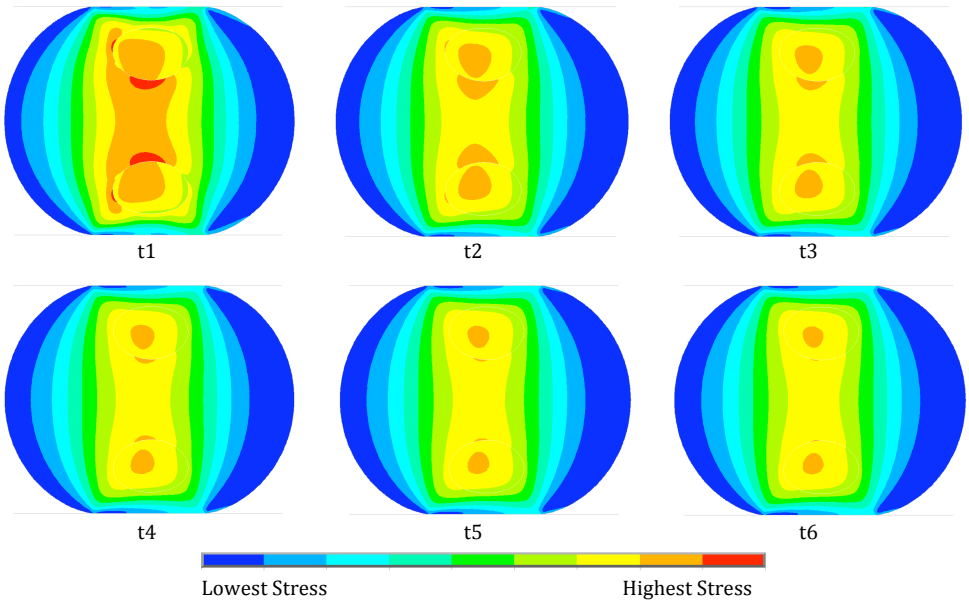

Figure 28: Stress Over Time – Typical Viscoelastic O-ring

Von Mises stress decay over time for an o-ring made from viscoelastic material V5, with a material inset with an elastic modulus of 3.0-MPa from Group 1 simulations. t_1 = 0-days, t_2 = 3.5-days, t_3 = 10.3-days, t_4 = 31-days, t_5 = 66-days, t_6 = 100-days. Stored energy in o-ring decreases from t_1 to t_6.

In order to counteract this loss of stored energy over time and decrease in sealing pressure, the use of adaptive-stiffening materials is proposed. The motivation behind the concept of utilizing adaptive material behaviors in seal designs stems from Klamecki et al. [20]. While there is no readily available material at this time that can demonstrate the material behavior being suggested, a material exhibiting reverse viscoelastic decay is proposed for development based on its usefulness as demonstrated in the numerical simulations and results to be described.

The material models proposed have an initial elastic and shear modulus, E and G, corresponding to that of a linear material with an elastic modulus of 3.0-MPa. Three material models were created that demonstrate an increased shear modulus, $G(t)$, over time. After 100 days, the three material models have final elastic moduli of 3.1-MPa, 3.2-MPa, and 3.3-MPa. The material behavior is shown in Figure 29, and the Prony constants of the material model are presented in Table 20.

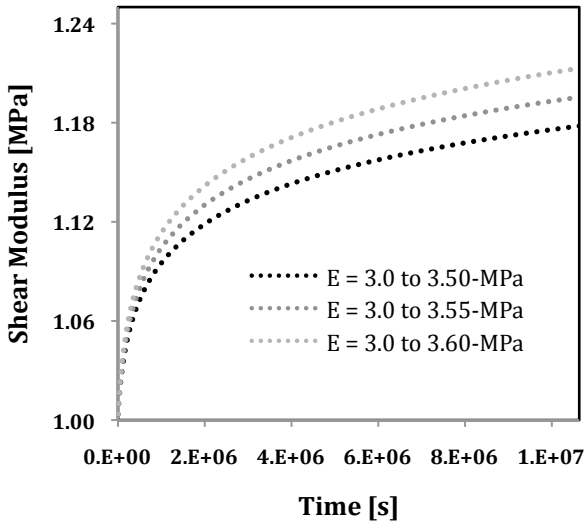

Figure 29: Adaptive-Stiffening Material Models
Proposed material behavior for o-ring insets to compensate for stored energy lost over time due to viscoelastic properties of elastomers.

Table 20: Prony Constants for Adaptive Stiffening Material Models

Prony Constants	*S6*	*S5*	*S4*
α_1	-6.777 E-11	-5.857 E-11	-5.878 E-11
τ_1	1	10	1
α_2	-6.777 E-11	-2.540 E-14	-5.878 E-11
τ_2	10	100	10
α_3	-1.416 E-17	-0.0363	-2.396 E-14
τ_3	100	1000.1	100
α_4	-0.0394	-0.0303	-0.0326
τ_4	1000.1	10000	1000.1
α_5	-0.0324	-0.0383	-0.0277
τ_5	10000	1.0 E5	10000
α_6	-0.0418	-0.0627	-0.0345
τ_6	1.0 E5	1.0 E6	1.0 E 5
α_7	-0.0677	-0.0259	-0.0568
τ_7	1.0 E6	1.0 E7	1.0 E6
α_8	-6.777 E-11	-5.857 E-11	-0.0235
τ_8	1.0 E7	1	1.0 E7

All materials used in this set of numerical simulations are presented in Table 21. Material L1 represents a linear material model with an elastic modulus of 3.0-MPa. Materials V6, V5, and V4 represent common elastomer materials with initial elastic moduli of 4.0-MPa, 3.8-MPa, and 3.6-MPa respectively. After 100 days, due to viscoelastic decay, these materials have elastic moduli of 3.2-MPa, 3.1-MPa, and 3.0-MPa respectively. Materials S4, S5, and S6 demonstrate adaptive-stiffening, i.e. an increasing shear modulus over time. Each material model has an initial elastic modulus of 3.0-MPa, but the elastic modulus increases over time to 3.1-MPa, 3.2-MPa, and 3.3-MPa respectively.

The different o-ring designs investigated, and the group designations, are listed in Table 22.

Table 21: Time-Dependent Material Properties

Material	E_o [MPa]	G_o [MPa]	E at 100-days [MPa]	G at 100-days [MPa]
L1	3.0	1.003	3.0	1.003
V6	4.0	1.338	3.2	1.070
V5	3.8	1.271	3.1	1.037
V4	3.6	1.204	3.0	1.003
S6	3.0	1.003	3.60	1.201
S5	3.0	1.003	3.55	1.186
S4	3.0	1.003	3.50	1.169

All material models had a Poisson's Ratio of $\nu = 0.495$.

Table 22: Viscoelastic Simulation Groups

Simulation Group	*Materials [Main O-ring / Inset]*
Group 1	V6 – L1
	V5 – L1
	V4 – L1
Group 2	V6 – S6
	V6 – S5
	V6 – S4

7.2.1. Results – Stress Over Time

Figure 28 presented earlier showed contour plots of Von Mises stress over time from the o-ring design V5-L1 from the Group 1 simulations. The strain energy content of the entire seal, which is directly related to the state of stress of the seal, decreases over time due to the viscoelastic properties of the main o-ring material. For comparison, the decrease in energy content is quantified by the size of the red and orange contours (the highest energy regions) from t_1 = 0-days, to t_6 = 100-days after compression. While the inset regions in these simulations do not have time-dependent decaying properties, the viscoelastic properties of the main o-ring material dominate, and there is a decrease in the overall state of stored energy across the seal, which is shown by the decrease in the size of the orange contour regions.

Figure 30 presents contour plots of Von Mises stress over time for the o-ring design V6-S5 from the Group 2 simulations, which were performed on the same seals, with the linear and time-independent properties of the inset regions changed to materials that stiffen slightly over time. From t_1 to t_5, the energy in the seal decreases, represented by the decrease in size of the red and orange contours. From t_5 to t_6 however, the orange contours maintain their size. That the size of the orange contours is unchanged for this period of time demonstrates the effect the adaptive material inset has on the seal.

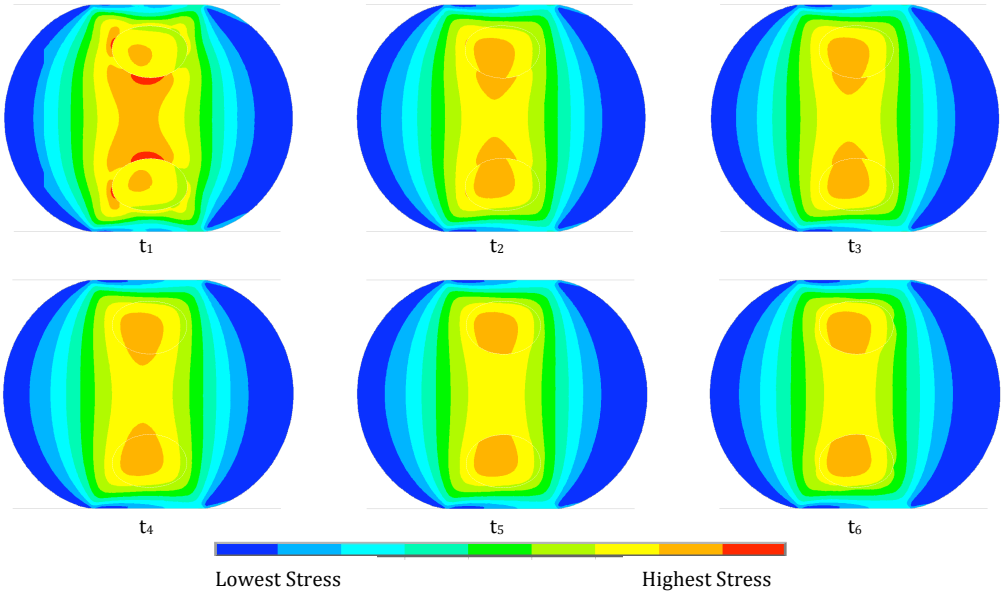

Figure 30: Stress Over Time – O-ring with Adaptive-Stiffening Inset
Von Mises stress decay over time for an o-ring made from viscoelastic material V6, with an inset of material S4 that exhibits adaptive-stiffening. t_1 = 0-days, t_2 = 2-days, t_3 = 4-days, t_4 = 8-days, t_5 = 18-days, t_6 = 100-days. Stored energy in o-ring decreases from t_1 to t_5, but reverses, and increases very slightly from t_5 to t_6.

Imaging software was used to quantify the change in size of the highest regions of Von Mises stress as designated by the red and orange contours in the plots shown in Figure 28 and Figure 30. The number of pixels of the orange and red bands were counted for each time, t_1 to t_6, and used to determine how much of the initial stress remained over time. The data, presented in Table 23, shows that the viscoelastic o-ring design, V5-L1, experienced a continuous decrease of stress over time, from 100% at t_1, to only 8% at t_6 = 100-days. The o-ring design with the stiffening inset, V6-S4, showed a decreasing stress from 100% at t_1 to 50% at t_5 = 18-days. In contrast, a slight increase of stress was seen over the remaining

time, as the stress at t6 = 100-days was 52% of the maximum at initial compression. This is due to the continual stiffening of the inset region.

Table 23: Stress Over Time

Time	*Pixels of high σ_{VM}*		*Stress Over time*	
	V5 - L1	V6 - S4	V5 - L1	V6 - S4
t_1	94953	55635	100%	100%
t_2	30491	36588	32%	66%
t_3	17366	33953	18%	61%
t_4	11322	31477	12%	57%
t_5	8468	28024	9%	50%
t_6	7419	28758	8%	52%

7.2.2. Results – ESED Over Time

As described previously, ESED over time was monitored in three regions of the o-ring cross-section. It should be noted that the ESED plots that are presented here are actual strain energy density values at the regions specified in the o-ring cross-section, and are not representative of the entire energy content of the seal, i.e. the ESED intensity, as was quantified in previous sections.

ESED values for the three regions described in Figure 26 were plotted over time for the different o-ring designs. Consistently, o-ring designs made from viscoelastic materials from Group 1 demonstrated exponentially decaying levels of ESED in all three regions. O-ring designs made from viscoelastic materials with adaptive-stiffening insets from Group 2 show varying degrees of ESED change over time for the different regions, as will be shown in further detail.

In Figure 31, ESED in the o-ring just outside the inset boundary is plotted over time for six different o-ring designs. For the Group 1 simulations, ESED decayed logarithmically over time, similar to the logarithmic decay of the shear modulus, *G(t)*. The o-ring made of the stiffest material, V6, exhibited the highest amount of stored energy, while the o-ring modeled from the least stiff material, V4, demonstrated the lowest amount of strain energy.

Since the inset region is unchanged in this group of simulations, it is expected to have the same effect on all three different o-ring designs.

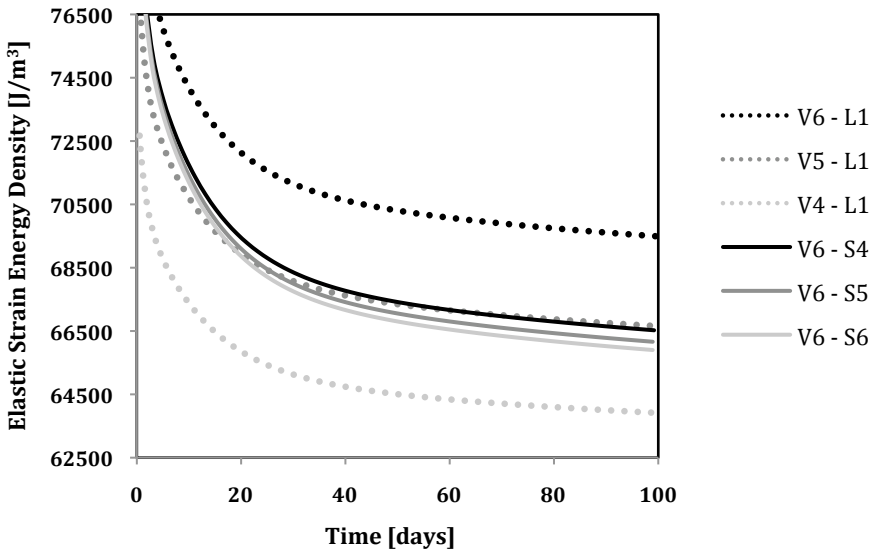

Figure 31: ESED Over Time – Sub-inset

As can be seen in Figure 31, the o-ring designs from Group 2 show a similar shape of ESED decay over time to those designs of Group 1. However, when the Group 2 designs are compared to the design of V6-L1, they all show a lower amount of ESED, which shows that the viscoelastic properties of the main o-ring material dominate, and in this region of the o-ring, there is still an overall decrease in stored energy over time.

ESED values at a point in the middle of the o-ring are plotted over time for the six o-ring designs in Figure 32. All designs from Group 1 show an exponential decay in ESED over time. As expected, the o-ring design V4-L1 demonstrates the lowest stored energy in the seal over time, as it had the lowest elastic modulus of all the designs. For the designs of Group 2, ESED is shown to increase over time. In this region, the viscoelastic properties of the main o-ring no longer dominate, but instead, the effect of the stiffening inset not only maintains the amount of strain energy, but also increases it as time moves forward. The o-ring design, V6-S6, had the largest stored energy over time as was expected since its inset demonstrated the largest amount of stiffening over time, increasing from 3-MPa, to 3.3-MPa.

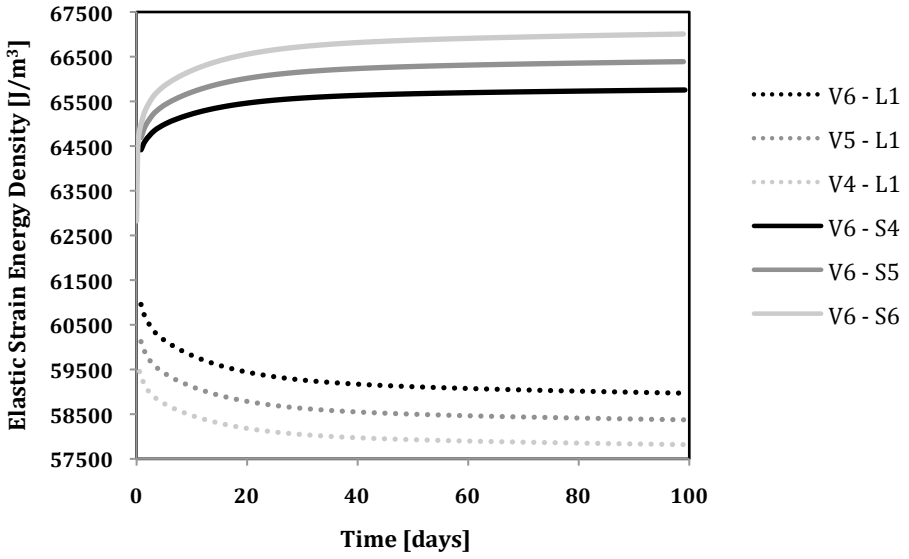

Figure 32: ESED Over Time – Mid O-ring

Figure 33 shows ESED over time in a region in the middle of the inset area of the o-ring. For the Group 1 designs, ESED decays exponentially. Although the properties of the inset material do not change over time for the Group 1 o-ring designs, the viscoelastic behavior of the main o-ring still dominates, and causes a decrease in energy in this region. For the o-ring designs from Group 2, the stiffening behavior of the insets causes an increase in the amount of energy stored in this region, as is expected. This increased strain energy content in the inset region of the seal has the effect of raising the overall strain energy content of the entire seal.

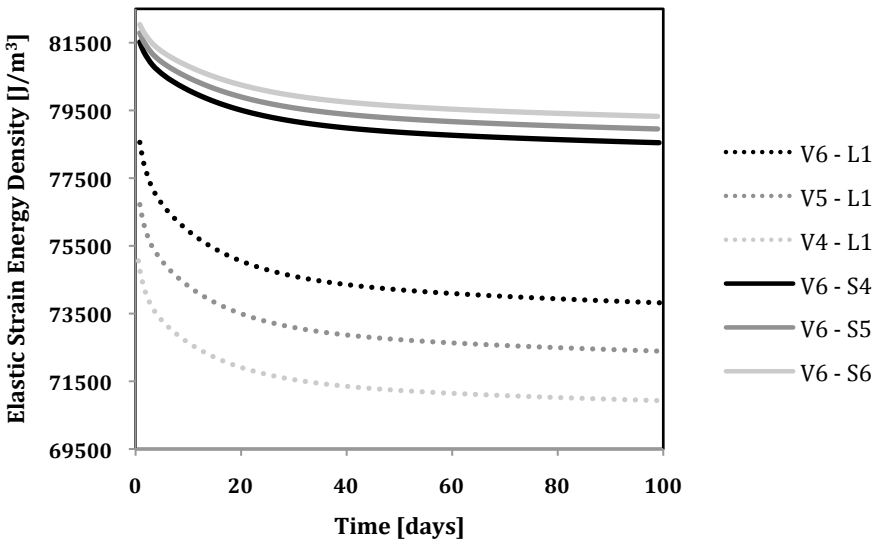

Figure 33: ESED Over Time – Mid Inset

The beneficial effect of the stiffening inset in the o-ring designs of Group 2 can be better appreciated by observing maximum contact pressure over time. As indicated earlier in Figure 26, the maximum contact pressure was monitored over time at the center of the contact area between the deformed o-ring seal and gland.

Changing sealing pressure over time for all the o-ring designs of Group 1 and Group 2 was plotted and is shown in Figure 34. As seen in the experimental results described in Section 5, contact pressure for the Group 1 designs, which is directly proportional to the measured sealing force, decay logarithmically over time. The o-ring design V6-L1, the o-ring with the highest initial stiffness, demonstrated the highest contact pressure of the Group 1 designs. O-ring design V4-L1 demonstrated the lowest contact pressure, as was expected because it had the lowest initial elastic modulus.

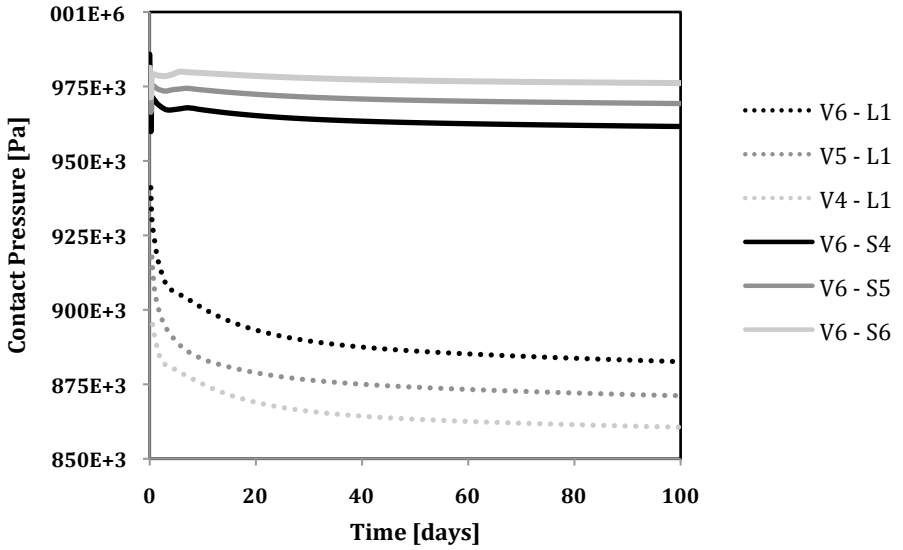

Figure 34: Contact Pressure Over Time

The Group 2 o-ring designs also exhibit contact pressures that decay over time. However, the attractive results are 1) the increase in contact pressure when compared to the designs of Group 1, and 2) the decrease in rate of loss of contact pressure over time. O-ring design V6-S4 maintained a maximum contact pressure of 9.71-MPa after 1-day, and a maximum contact pressure of 9.61-MPa after 100-days. The highest sealing pressures were seen in design V6-S6: 9.80-MPa after 1-day, and 9.76-MPa after 100-days. This result is expected, as the inset in design V6-S6 exhibited the largest adaptive stiffening, which results in a higher strain energy content in the entire seal. Table 24 shows the maximum sealing pressure of the seals after 1-day, and 100-days, held under a fixed displacement.

Table 24: Sealing Pressure after 100 days

O-ring Design	*CP – Day 1 [Pa]*	*CP – Day 100 [Pa]*	*Differential [Pa]*	*Decrease*
V6 - L1	924691	882682	42009	4.54%
V5 - L1	908205	871267	36938	4.07%
V4 - L1	895103	860624	34479	3.85%
V6 - S4	970638	961583	9055	0.93%
V6 - S5	975127	969265	5862	0.60%
V6 - S6	979098	976144	2954	0.30%

8. Conclusions

The results documented in this work have demonstrated that strain energy is a useful design parameter in developing new seal designs for controlled and improved performance. Numerical studies and experimental methods were both utilized to produce results that showed how variations in material properties and material behavior across an o-ring cross section can produce desired reductions in strain energy. The later numerical results also demonstrated methods of utilizing adaptive material behavior in order to combat the long-term viscoelastic properties of elastomer materials, and maintain higher sealing pressures than baseline single material o-ring designs.

Numerical simulations with linear material behavior models described in Section 4 showed that inset placement and stiffness can be important design parameters for o-ring seals. It was shown from the two different groups of o-ring designs, (those where the inset was offset from the surface, and those where the inset was just below the o-ring surface,) that the amount of elastic strain energy density content in the seal and the maximum sealing pressure can be managed. These quantities can be controlled by modifying material properties in different regions of the seal. The placement of the region of material behavioral changes can be optimized for the sealing application.

The concept of improving seal performance by decreasing strain energy content was also validated by experimental methods. As described in Section 5, realistic experimental o-ring seals that were created with internally distributed modified material properties demonstrated two modes of improved performance. First, a decreased rate of sealing force decay of up to 46% was observed in the designs with the least amount of strain energy, which were the seal designs created with the largest soft inset regions. Second, in the same experimental seal designs, a decrease in the amount of permanent deformation, i.e. compression set, was measured in all modified designs. Compression set was measured at 95% for baselines designs, while modified designs exhibited compression set values of 87%, 78%, and 67%.

The numerical simulations conducted with linear material models and experimental methods both demonstrated the potential for improved long-term seal performance. However, these improvements came at the expense of a decrease in maximum potential sealing force for modified sealing designs. To combat this undesired result in the seal designs, further numerical studies were conducted that investigated the effects of using materials with non-linear and adaptive behavior in o-ring insets.

As described in Section 6, material models were created where the degree of the rubber's natural strain-stiffening response was modified to occur at lower strain values. In most of the material models developed, it was shown that any increases in the maximum potential sealing pressure were accompanied by even greater increases in the strain energy content of the seal. Noteworthy trends were identified when modifications in the biaxial and shear strain-stiffening responses of the material models were included. It was observed that when only the material's biaxial strain-stiffening response was increased, the maximum potential sealing force increased larger amount than the strain energy content of the seal. Similar effects were seen when only the material's shear strain-stiffening response was increased. In many of the initial material models, strain energy would increase up to 13% more than contact pressure, an undesired result. In the designs with isolated material behavioral responses, maximum sealing pressure increased up to 1.7% more than that of the strain energy density content in the seal. This increase is small, and requires further study to identify different material modifications that can result in greater sealing pressure increases, while maintaining lower strain energy content.

Finally, Section 7 described a mode of adaptive material behavior to compensate for the viscoelastic effects of rubber materials. While minimizing strain energy content in the seal was the design parameter in the other work described, this level of strain energy content realized in the seal then needs to be maintained over time. Stored energy in the seal is the main contributor to the ability of the seal to perform its sealing function.

Simulation results showed that materials that exhibit an increasing shear modulus behavior over time, and adaptive stiffening, are a viable approach to decreasing the decay of contact

pressure over time. Material models were created that displayed reverse viscoelastic behavior and seal designs were proposed where these materials were utilized as insets in the o-ring seal. Numerical simulations showed that designs with typical viscoelastic behavior would exhibit sealing pressure values 5% less than their initial values after 100-days under compression. The modified o-ring designs made of the same viscoelastic material, but with small inset regions that employed an adaptive-stiffening behavior, all demonstrated less than 1% loss of sealing pressure over the same 100-days under compression.

The implications of the final group of numerical simulations are great. They are a step toward an overall research area investigating employing adaptive materials to realize improved seal performance over time. An o-ring that can naturally counteract the onset and growth of permanent deformation will be very advantageous in decreasing the amount of maintenance required in fluid power systems.

9. Recommendations

Based on experimental work and numerical simulations, the following recommendations are made for future work relating to the problem of improving seal design based on adaptive material behavior.

First, in future experimental testing, it is recommended that:

1) Multiple specimens should be tested for the each testing procedure to ensure repeatability of seal response based on designed material behavior.
2) Testing conditions be monitored to ensure comparable environmental conditions, such as room temperature and humidity.
3) Samples should be evaluated with an initial heat cycle prior to aging in order to determine the relaxation effect [29].
4) Samples should be mechanically over-strained for a short time period before returning to the application strain level can help gain a more accurate picture of long-term compression set effects [12].

The intent of these recommendations is to avoid some of the inconsistency in stress relaxation testing that was seen in Section 5 this work. Also, the compression set measurements that were conducted were only for a short period of time in keeping with ASTM recommendations. In order to demonstrate the potential long-term improved sealing performance, it is recommended that more advanced age-testing be performed in order that seal designs being tested can approach their long-term equilibrium values, i.e. the point where the continuing permanent deformation becomes negligible, as this would provide a more concrete comparison of the long-term effects and viability of proposed seal designs.

Additional recommendations include:

1) Create new experimental o-ring and seal samples made from rubber materials optimized for industrial sealing applications.

2) Apply the design rules presented in this work to more complex problems, where different loading conditions and working fluid pressure is considered.
3) Investigate current materials, modifying material properties, and methods of designing materials, that demonstrate the advantageous adaptive-stiffening described in this work.
4) Investigate the usage of auxetic material behavior, i.e. Poisson's ratio $\nu < 0$, in varying regions across the seal cross-section for potential beneficial effects balancing increased maximum potential sealing pressure with maintained lower strain energy levels as suggested in the results presented in this work.
5) Investigate the long-term potential cost savings that improved sealing performance can contribute to different industries.
6) Utilize the design rules presented in this work to the design of different elastomer products that can also benefit from improved long-term performance of rubber materials. Examples include other types of elastomer seals, gaskets, dampers, shock absorbers, and sponges [30].

The additional recommendations are made with the intent of expanding the implications of this work. The specific recommendation of investigating the use of auxetic materials is made because some initial investigation was conducted while conducting this research. However, not enough results were generated to identify any convincing trends in material behavior, and thus no conclusive results are presented. Also noted is that the results of this work are not restricted to sealing applications, but have implications in many other areas where elastomer materials and viscoelastic polymers are used.

10. References

1. Dichtomatik Americas, "O-ring Handbook," http://www.dichtomatik.us/Literature/O-ring-Handbook.aspx. Accessed May 30, 2010.
2. Allorings.com, "O-ring Failure Analysis," http://www.allorings.com/failure.htm. Accessed: May 18, 2010.
3. Sefkow, R. B., 2007, "Improving the Predicted Performance of O-rings Over Time Via Material Design," MSME thesis, University of Minnesota, Minneapolis, MN.
4. Maciejewski, N. J., 2007, "The Analysis and Reduction of Compressive Set in O-rings," MSME thesis, University of Minnesota, Minneapolis, MN, USA.
5. Chou, P., Pagano, N., 1992, "Elasticity: Tensor, Dyadic, and Engineering Approaches," Dover Publications, Inc., Mineola, New York, USA.
6. Bergström, J. S., Boyce, M. C., 1998, "Constitutive Modeling of the Large Strain Time-Dependent Behavior of Elastomers," Journal of the Mechanics and Physics of Solids, **46**(5), pp. 931-54
7. Bower, Mark V., Ledbetter, Frank E., 1991, "Predicting compression set in elastomeric materials," Mechanics of Materials 11 (1991) 177-197.
8. Dragonni, E., Strozzi, A., 1988, "Analysis of an Unpressurized, Laterally Restrained, Elastomeric O-ring Seal," ASME J. Tribology, **110**(3), pp. 193-200.
9. Green, I., English, C., 1992, "Analysis of Elastomeric O-ring Seals in Compression Using the Finite Element Method," Tribology Transactions, **35**(1), pp. 83-88.
10. Warren, W. E., Weese, J. A., 1997, "The Deformation of O-rings Compressed by Smooth Rigid Plates," ASME J. Energy Resource Technology, **119**(2), pp. 73-80.
11. Akisanya, A. R., Hitchcock, G. R., Thompson, D. S., 2001, "The Deformation of a Dual-Elastomer Seal," Proc. Institute of Mechanical Engineering, Part L: Journal of Materials: Design and Applications, **215**, pp. 29-40.
12. Gillen, K.T., Bernstein, R., Wilson, M. H., 2004, "Predicting and confirming the lifetime of o-rings," Polymer Degradation and Stability, **87**, pp. 257-270.
13. Bernstein, R., Gillen, K.T., 2009, "Predicting the lifetime of fluorosilicone o-rings," Polymer Degradation and Stability, **94**, pp. 2107-2113.

14. Bigg, D. M., Heater, K. J., Skidmore, T. K., 2005, "Hydrocarbon Stability of Perfluorinated Polyether Rubbers at Elevated Temperatures," Polymer Engineering and Science, **45**(12), pp. 1622-1629.
15. Andrews, R. D., Tobolsky, A. V., Hanson, E. E., 1946, "The Theory of Permanent Set at Elevated Temperatures in Natural and Synthetic Vulcanizates," Journal of Applied Physics, **17**(5), pp. 352-361.
16. Bergström, J. S., Boyce, M. C., 2000, "Large Strain Time-Dependent Behavior of Filled Elastomers," Mechanics of Materials, **32**(11), pp. 627-44.
17. Achenbach, M., 2000, "Service Life of Seals – Numerical Simulation in Sealing Technology Enhances Prognoses," Computational Materials Science, **19**(1-4), pp. 213-222.
18. Nilkanth, Vinay, Campbell, Alan, 1991, "Nonlinear Finite Element Analysis in the Closed Loop Seal Design Cycle," SAE Technical Paper Series, 42nd Annual Earthmoving Industry Conference.
19. Calvert, C., Tirovic, M., Stolarski, T., 2002, "Design and development of an elastomer-based pneumatic seal using finite element analysis," Proceedings of the Institution of Mechanical Engineers, Part J: Journal of Engineering Tribology, **216**(3), pp. 127-138.
20. Sefkow, R., Maciejewski, N., Klamecki, B., 2009, "Improving Long-term Performance of O-rings through Material Behavior Design," ASME Journal of Tribology, **131**, pp. 042203-1 – 042203-9.
21. Hertz Jr., D. L., 1979, "O-rings for Low Pressure Service," Machine Design, Penton/IPC Inc., Cleveland, OH.
22. ASTM D412-06, Standard Test Methods for Vulcanized Rubber and Thermoplastic Elastomers – Tension.
23. ASTM D1415-06, Standard Test Methods for Rubber Property – International Hardness
24. ASTM D395-03, Standard Test Methods for Rubber Property – Compression Set.
25. "Theory Reference for ANSYS and ANSYS Workbench," 2007, ANSYS, Inc. Southpointe 275 Technology Drive Canonsburg, PA 15317, http://www.ansys.com
26. McCulloch, Euan, 2008, "Experimental and Finite Element Modeling of Ultrasonic Cutting of Food," Doctoral Thesis, University of Glasgow, Scotland.
27. Drozdov, A. D., deClaville Christiansex, J, 2005, "Constitutive equations for the nonlinear elastic response of rubbers," *Acta Mechanica*, **185**(1-2), pp. 31-65.

28. Chen, T., 2000, “Determining A Prony Series for A Viscoelastic Material from Time Varying Strain Data,” US Army Research Laboratory, NASA Center for Aerospace Information.
29. Tuckner, P., 2000, “Compression Stress Relaxation Test Comparisons and Development,” SAE Technical Paper Series, 2000-01-0752.
30. Ballato, A., 2010, “Poisson’s Ratios of Auxetic and Other Technological Materials,” IEEE Transactions on Ultrasonics, Ferroelectrics, and Frequency Control, **57**(1).

Appendices

A. Experimental Supplies

Table 25 lists the commercially available items that were used in conducting the various experiments in this work.

Table 25: Experiment and Testing Supplies

Item	*Use*	*Vendor*	*Part Number*
Flexane® 80 Liquid	Primary o-ring molding material	Grainger	5A460
Devcon Liquid Release Agent	De-molding aid	Grainger	3DPJ6
2-mm CS, 35-mm ID 70A o-ring	As o-ring inset	RT Dygert	1457N70
3-mm CS, 34-mm ID 70A o-ring	As o-ring inset	RT Dygert	2692N70
4-mm CS, 33-mm ID 70A o-ring	As o-ring inset	RT Dygert	1279N70
0.5-in Ball-end end mill	For mold fabrication	Walter Hammond	C42657
13/32-in Unthreaded round spacer	For compression set test	McMaster	92510A274

B. Technical Data Sheet: Flexane® 80

Devcon®

Technical Data Sheet

8/18/2004

Flexane® 80 Liquid

Description: A medium-viscosity castable, nonshrinking urethane compound.

Intended Use: Reproduce low- to medium-volume or discontinued rubber parts; form flexible molds and nonscratching holding fixtures/linings; encapsulate wire and electronics subject to impact, vibration, expansion, and contraction.

Product features:
10-hour demolding time
Room temperature curing urethane/no heat required
Mixes and pours easily

Limitations: None

Typical Physical Properties:

Technical data should be considered representative or typical only and should not be used for specification purposes.

Cured 7 days @ 75° F

		TESTS CONDUCTED
Color	Black	
Mix Ratio	77resin: 23 curing agent (by wt.)	Dielectric Strength, volts/mil ASTM D 149
Mixed Viscosity	10,000 cps	Tensile Strength (Urethanes) ASTM D 412
% Solids by Volume	100	Cured Hardness Shore D ASTM D 2240
Specific Volume	26.5 in.(3)/lb.	Cure Shrinkage ASTM D 2566
Cured Shrinkage	0.0018 in./in.	Tear Resistance ASTM D 624
Maximum Operating Temperature	Dry: 180°F; Wet: 120°F	Maximum Elongation ASTM D 412
Coverage / lb	106 sq.in./lb. @ 1/4"	
Cured Hardness	87A	
Dielectric Strength	350 volts/mils	
Demolding Time	10 hrs.	
Tensile Strength	2,100 psi	
Tear Resistance	350 pli	
Maximum Elongation	650%	
Abrasion Resistance	285 mg loss per 1,000 revolutions (H 18 wheel/1,000 cycles)	
Functional Cure	16 hours	
Pot Life	30 min. @ 75°F	

Surface Preparation:

For METAL SURFACES, thoroughly clean area to be repaired, rebuilt, or lined with Devcon® Cleaner Blend 300. Remove any oil, grease, or dirt. Roughen surface by grinding with a coarse wheel or an abrasive disc pad. To prime this surface, apply a coat of Devcon FL-10 Primer and allow to dry tack-free for 15 minutes. If the metal surface requires maximum tear resistance or is exposed to moisture, or if submerged in water, use Devcon® FL-10 and Devcon® FL-20 Primer.

For RUBBER SURFACES, thoroughly clean area with an abrasive pad and Devcon® Cleaner Blend 300. Surface can also be roughened with a grinding wheel so that it is coarse and free from oil and dirt that may clog the "pores" of the rubber. Wipe or roughen surface with Cleaner Blend 300 until the cloth no longer picks up the color of the rubber. The rubber should appear new or deeper in color. To prime this surface, apply a coat of Devcon® FL-20 Primer and allow to dry tack-free for 15-20 minutes. Use Devcon®FL-40 Primer on "hard-to-bond" rubber surfaces as this gives ultimate peel resistance. Multiple coats may be necessary for porous rubber surfaces.

For MAXIMUM ADHESION, sandblast the surface with an angular abrasive until a minimum depth profile of 2-3 mils is met. Blast to near-white finish specification SSPC-SP5 (Steel Structure Painting Council). Prime surface immediately after sandblasting to prevent oxidation.

Mixing Instructions:

---- To ensure proper cure speeds and hardness, mix Flexane at a temperature between 65°F-85°F. ----

1.Add hardener to resin.
2.Vigorously mix with screwdriver or spatula for two minutes, while continuously scraping material away from sides and bottom of container.
3.Transfer the mixed material to the plastic container (included in kit).
4.Wipe spatula clean, and stir again for two more minutes.

FOR 400ML CARTRIDGES:

ITW Devcon, 30 Endicott Street, Danvers, MA 01923 Tel:(978) 777-1100 Fax:(978) 774-0516 www.devcon.com

Application Instructions:

1.Attach mix nozzle to cartridge
2.Follow application instructions; no mixing is required.

FOR 10LB. UNITS:
Use a propeller-type Jiffy Mixer Model ES on an electric drill.

Mix until color is uniform and consistent (approx 4-6 min.).

NOTE: Completely submerge propeller, otherwise large amounts of air will be added resulting in air bubbles on the finished product's surface.

---- FOR MAXIMUM ADHESION, apply a suitable Devcon primer to all substrates prior to application. ----

Metals	FL-10 Primer
Rubber	FL-20 Primer
Wood	FL-20 Primer
Fiberglass	FL-20 Primer
Concrete	FL-20 Primer
Rigid Plastics	FL-20 Primer (2 coats)

1.Brush a thin coat of Flexane over the substrate, then pour from one side of the mold to the other side, so as to evacuate any air as the Flexane fills the area.
2.Gently blow hot air over the finished surface to ensure a perfect mold with no blow holes or air entrapment. Use a hot air gun and gently wave over the surface to break all the air bubbles.
3.Allow to cure ten (10) hours before returning equipment to light service. The repair may then be ground flush using a 24 or 36 grit sanding disc. Do not overheat the work surface. Full cure takes seven (7) days @ 70°F.

ADDITIONAL INFORMATION
Flex-Add Flexibilizer is used with Flexane 80 Liquid to produce a urethane with a durometer below 80A. This allows for custom mixing of urethanes for specific applications requirements. (See Flex-Add TDS for further information)

Flexane Accelerator is used to increase Flexane's cure speed at temperatures as low as 32°F. One-half tsp. (2 gms) of Accelerator reduces the cure time of 1 lb. of Flexane by 50%. Use 2 tsp. or less of Accelerator for each 1 lb. of Flexane. See Flexane Accelerator TDS for further information.

Storage: Store at room temperature.

Compliances: None

Chemical Resistance: *Chemical resistance is calculated with a 7 day, room temp. cure (30 days immersion) @ 75°F)*

1,1,1-Trichloroethane	Poor	Phosphoric 10%	Very good
Aluminum Sulfate 10%	Very good	Potassium Hydroxide 40%	Very good
Cutting Oil	Fair	Sodium Hydroxide 50%	Very good
Gasoline (Unleaded)	Poor	Sodium Hypochlorite	Very good
Hydrochloric 10%	Very good	Xylene	Poor
Hydrochloric 36%	Very good		
Isopropanol	Poor		
Methyl Ethyl Ketone	Poor		

Precautions: Please refer to the appropriate material safety data sheet (MSDS) prior to using this product.
For technical assistance, please call 1-800-933-8266
FOR INDUSTRIAL USE ONLY

Warranty: Devcon will replace any material found to be defective. Because the storage, handling and application of this material is beyond our control, we can accept no liability for the results obtained.

Disclaimer: All information on this data sheet is based on laboratory testing and is not intended for design purposes. ITW Devcon makes no representations or warranties of any kind concerning this data.

Order Information:
15800 1 lb.
15810 10 lb.

ITW Devcon, 30 Endicott Street, Danvers, MA 01923 Tel:(978) 777-1100 Fax:(978) 774-0516 www.devcon.com

C. O-ring Casting Standard Operating Procedure

Ensure ambient temperature is 55-90°F

Items Needed
- Casting Agent
- Resin
- Mold
- Mixing container
- Scale
- Heat gun
- Mold release agent

Steps
- Thoroughly clean mold halves. Remove any oil, grease or dirt.
- Apply liquid release agent to mold
- Place o-ring inset into mold if applicable
- Determine proper casting-agent to resin ratio
- Add casting agent to resin.
- Vigorously mix for at least 2-minutes.
- Pour mix into mold in a very thin stream to eliminate air pockets forming.
- When filled halfway, gently blow hot air over surface (use a hot air gun and gently wave over the surface to break all the air bubbles.)
- Wipe spatula clean and stir again for two minutes.
- Pour into both mold halves.
- Brush a thin coat of Flexane over mold, then pour from one side of the mold to the other side to evacuate any air as the compound fills the volume.
- Gently blow hot air over the finished surface to ensure a perfect mold with no blow holes or air entrapment (use a hot air gun and gently wave over the surface to break all the air bubbles.)
- Let rest for at least 30-minutes before closing mold halves.
- Add a final thin stream of mixture to ensure mold is slightly over-flowing, which will assist in bonding the mold halves.
- Clamp mold close, and flip every 5-minutes for 30-minutes to ensure an even mold cure.
- After first 30-minutes, flip mold every 15-minutes until 2-hours after cure.
- Allow to cure 10-hours before de-molding.
- Allow to sit 7-days to reach full 100% cure.

Last updated: March 8, 2010

D. Elastomer Materials: Sample Test Data

A fair amount of deviation was seen in the testing data from the o-ring samples made from the Devcon Flexane® product. While it is posited that some of the deviation is a result of the non-optimized rubber compound application and imperfect molding procedure, it is noted that even industrial rubber compounds that are optimized for sealing applications tend to display a certain amount of deviation when undergoing mechanical testing.

Table 26: Tensile Tests – Sample Data for Nitrile Rubber

	3895A		***3895B***		***3895C***	
Strain	**Stress [MPa]**	**Deviation**	**Stress [MPa]**	**Deviation**	**Stress [MPa]**	**Deviation**
10%	0.89	0.06	0.90	0.06	0.89	0.01
20%	1.37	0.07	1.38	0.06	1.38	0.02
30%	1.73	0.07	1.74	0.05	1.73	0.02
40%	2.05	0.09	2.03	0.05	2.02	0.02
50%	2.36	0.12	2.28	0.02	2.28	0.03
100%	4.41	0.29	4.00	0.03	3.71	0.07
150%	7.70	0.52	6.70	0.00	5.56	0.11
200%	11.39	0.62	9.90	0.03	7.57	0.10
250%	14.55	0.55	12.16	0.00	8.83	0.09
300%	17.06	0.39	13.38	0.05	9.35	0.12
350%	17.88	1.25	14.12	0.10	9.57	0.00